A robotic device for MRI-guided prostate brachytherapy

Vera Lagerburg

A robotic device for MRI-guided prostate brachytherapy

Een robot voor prostaat brachytherapie onder MRI-geleide
(met een samenvatting in het Nederlands)

Proefschrift ter verkrijging van de graad van doctor aan de
Universiteit Utrecht
op gezag van de rector magnificus, prof. dr. J.C. Stoof,
ingevolge het besluit van het college voor promoties
in het openbaar te verdedigen
op dinsdag 20 mei 2008 des ochtends te 10.30 uur

door
Vera Lagerburg
geboren op 6 september 1979 te Middenbeemster

Promotoren: Prof. dr. J.J. Battermann
Prof. dr. ir. J.J.W. Lagendijk
Co-promotor: Dr. ir. M.A. Moerland

Contents

Chapter 1

Introduction

1.1 Prostate cancer

The most recent figures from the Comprehensive Cancer Centres (CCC's) in the Netherlands show that 74.500 new cases of cancer were diagnosed in the Netherlands in 2005, 37.500 in men and 37.000 in women. 38.500 People died that year as a result of cancer. With 7.500 new cases in 2005 prostate cancer is the most common type of cancer in men (20% of total). Prostate cancer is mainly a disease of the elderly man, with more than 75% of new prostate cancers diagnosed in men older than 65 years. Since the beginning of the nineties the incidence in prostate cancer in men between 50 and 59 has increased remarkably. In addition to this change in incidence, there has been a change in prostate cancer stage at diagnosis. Especially localised prostate cancer is diagnosed more often, while the incidence of metastatic disease has decreased. These changes are mainly caused by the ability to measure the value of the Prostate Specific Antigen (PSA).

1.1.1 Diagnosis of prostate cancer

Prostate cancer rarely causes symptoms early in the course of the disease, because the majority of the tumours are located in the periphery of the gland, distant from the urethra (Chen *et al.*, 2000). Therefore suspicion of prostate cancer, resulting in a recommendation for prostate biopsy, is mostly raised by abnormalities found on Digital Rectal Examination (DRE) or by serum PSA

elevations. At present, transrectal ultrasound-guided (TRUS) needle biopsy is the most reliable method to diagnose prostate cancer.

TRUS-guided needle biopsy is, while inexpensive, an operator-dependent diagnostic test. The technique examines the prostate in different planes, one section at a time, such that a two-dimensional imaging procedure can be used to reconstruct a three-dimensional image. The whole gland is sampled in a systematic way, based on prostate anatomy and the location of most prostate cancers. Most centres currently use a sextant technique, but many centres are moving to more cores as routine (Raja *et al.*, 2006). However, the capsule is not visible by TRUS and therefore the diagnosis of extracapsular involvement is very difficult, with a specificity of detecting capsular infiltration of only 25% (Hsu *et al.*, 2006). The specificity of TRUS is being improved through the use of colour Doppler, power Doppler and three-dimensional ultrasonography, and contrast agents, with the aim of reducing unnecessary biopsies by using computational modelling (Remzi *et al.*, 2004; Teillac, 2004; Raja *et al.*, 2006). Current developments in taking biopsies include the development of MRI-guided biopsy (Beyersdorff *et al.*, 2005; Engelhard *et al.*, 2006; Susil *et al.*, 2006).

1.2   Treatment options

Different treatment possibilities are available for prostate cancer and the effectiveness depends, among other things, on the tumour stage (Vicini *et al.*, 1999; Weldon, 2002; Peschel and Colberg, 2003). For early stage prostate cancer possible treatment options are external beam radiation (RT), radical prostatectomy (RP), and permanent prostate brachytherapy (BT). Results of randomised trials between these three treatment options are lacking, but the freedom from biochemical recurrences (FBR) seems to be similar for RT, RP, and BT (Kupelian *et al.*, 2004; Potters *et al.*, 2004). The 10-year prostate-cancer-specific survival for the three treatments according to tumour grade are: 90 to 95% for grade 1, 70 to 90% for grade 2 and 40 to 70% for grade 3 (Lu-Yao and Yao, 1997). As treatment outcome is considered to be the same for all three treatment options, expected side effects and quality of life changes for the different treatment options can influence the treatment choice (Wei *et al.*, 2002; Miller *et al.*, 2005). For all three treatment options the decrease of quality of life after the treatment is only temporary. The baseline quality of life is mostly regained

at approximately six months after treatment. Regarding toxicity profiles there are some differences between the treatment options. In prostatectomy a risk for urinary incontinence exists of approximately 10 %, in external beam irradiation especially proctitis complaints (diarrhoea) occur (13 %) and in brachytherapy there is a risk of urinary retention of 6 % (Peschel and Colberg, 2003; Peeters *et al.*, 2006; Zelefsky *et al.*, 2007). For locally advanced tumours (with tumour extension outside the prostate capsule) only external beam irradiation is a treatment possibility. 5-Year absolute survival in these patients, treated only with external beam irradiation, is approximately 60 % (Bolla *et al.*, 2002).

1.2.1 Prostatectomy

Radical prostatectomy consists of surgical removal of the prostate and the seminal vesicles and can be performed by an open (retropubic and perineal) or a laparoscopic approach (Weldon, 2002; Peschel and Colberg, 2003; Damber and Khatami, 2005). Disadvantages of radical prostatectomy are the risk of incontinence and impotence. Depending on tumour stage, uni- or bilateral nerve sparing is possible to save potency. Erectile dysfunction after prostatectomy is, among other things, depending on age, baseline sexual function, smoking, and the surgeons skills in nerve sparing (Damber and Khatami, 2005).

1.2.2 External beam irradiation

With external beam irradiation the tumour is irradiated with a photon beam, delivered by a linear accelerator. Recently several groups have studied the effect of dose escalation (Khoo, 2005; Mangar *et al.*, 2005; Pollack *et al.*, 2006; Kuban *et al.*, 2008). To improve local control by escalating the dose, without increasing the dose to surrounding critical structures, intensity modulated radiation therapy (IMRT) has been implemented in many institutes. Prostate motion during radiotherapy (intra- and inter-fraction motion) makes it necessary to add a treatment margin to the radiation field, whereby the dose to the surrounding organs at risk should be taken into account. However, in case of small margins, the dose delivered to the GTV (gross tumour volume) can be less than the prescribed dose (Balter *et al.*, 1995b; Van Herk *et al.*, 1995). To follow prostate motion in time, gold markers can be implanted into the prostate as reference markers for the prostate motion (Dehnad *et al.*, 2003;

Van der Heide *et al.*, 2007). Other possibilities are the use of cone-beam CT (Smitsmans *et al.*, 2005) and in the future the MRI-accelerator (Raaymakers *et al.*, 2004; Lagendijk *et al.*, 2008).

1.2.3 Brachytherapy

Brachytherapy is the internal irradiation of the tumour with radioactive sources. In brachytherapy of prostate tumours it is possible to deliver an adequate radiation dose to the prostate while sparing critical surrounding organs like the neurovascular bundles, and the rectum (Merrick *et al.*, 2001; Stone and Stock, 2002; Merrick *et al.*, 2003b) due to the sharp dose gradient. Source placement precision is an important limiting factor for the optimisation of the dose distribution, since deviations from pre-planned positions may effect the planned dose significantly (Dawson *et al.*, 1994; Moerland *et al.*, 1997).

There are two major methods of prostate brachytherapy, permanent seed implant and temporary brachytherapy. Temporary brachytherapy can be separated in high dose rate (HDR) and pulse dose rate (PDR) brachytherapy (Gerbaulet *et al.*, 2002).

HDR brachytherapy uses radioactive sources with usually high activity and photon energy, e.g. Iridium-192. PDR brachytherapy uses sources with a lower activity. The sources are inserted in the prostate for a short time, using very tiny plastic catheters, for a short series of radiation treatments.

Examples of seeds used for permanent implants are Iodine-125 and Palladium-103. The insertion of needles for permanent seed delivery in prostate brachytherapy is currently done under ultrasound guidance (Holm *et al.*, 1983). In our institute the implant procedure is performed with patients placed in lithotomy position (Battermann, 2000). A Foley catheter is placed before the introduction of the needles. A rectangular template with 5mm spaced holes is positioned against the perineum. Two locking needles are inserted into the prostate, one on each side. Thereafter the needles are inserted parallel to each other and are used for the delivery of the Iodine seeds. Before the seeds are delivered, the position of the needles in the prostate is verified and adjusted if necessary. Two different techniques of delivering the seeds are applied at our institute, viz. manually using strands or automatically using loose seeds and the FIRST System (Nucletron, Veenendaal, The Netherlands). The seeds are delivered by

retracting the needle while the stylet remains at its position. After delivering of the seeds the needle and stylet are retracted.

1.3 MRI in prostate cancer

Visualisation is important in the process of detection, staging and treatment of prostate cancer. Compared with ultrasound, Magnetic Resonance Imaging (MRI) offers a better soft tissue contrast, which makes it possible to visualise structures inside the prostate (Cheng and Tempany, 1998; Husband *et al.*, 1998; Rasch *et al.*, 1999; McLaughlin *et al.*, 2005; Villeirs *et al.*, 2005b). Despite of this, the value of MRI in the detection, localisation, staging and treatment of prostate cancer is controversial. Detection accuracy varies widely among different studies (Sonnad *et al.*, 2001; Engelbrecht *et al.*, 2002). Part of these differences has been suggested to be related to reader experience (Yu *et al.*, 1997).

The combination of an endorectal coil with a surface coil can help to increase the diagnostic accuracy of MRI (Engelhard *et al.*, 2001). Wefer *et al.* (2000) compared the accuracy of endorectal MRI and MRS (Magnetic Resonance Spectroscopy) with that of sextant biopsy for the localisation of prostate cancer and concluded that MRI and MRS were each more sensitive but less specific than biopsy for sextant localisation of prostate cancer. In the apex they were both more accurate than biopsy. Mullerad *et al.* (2005) conclude that MRI contributes significant incremental value to DRE and TRUS biopsy findings. In patients with an elevated PSA and negative biopsy, MRI can also offer additional value, because of a higher sensitivity for detection of prostate cancer compared with DRE of TRUS in this patient group (83% vs 33% vs 33%) (Beyersdorff *et al.*, 2002).

New developments in MRI, such as higher magnetic field strengths, MRI spectroscopy, and increasing reader experience, will increase the importance of MRI in prostate cancers. In many centres MRI is already used as a (complementary) diagnostic tool. For the evaluation of permanent prostate brachytherapy MRI is also of value (Moerland *et al.*, 1997). Currently postimplant dosimetric evaluation is mostly done on radiographs or CT (Computed Tomography), but these give no information regarding the position of the seeds relative to

the prostate. With a combination of radiographs and MRI accurate evaluation of the implant is possible. Also during treatment MRI gains importance. D'Amico *et al.* (1998) e.g. perform MRI-guided brachytherapy in an open MRI scanner. Because of the poor image quality of the low field scanners, other groups are developing MRI-guided tools for closed bore scanners. Beyersdorff *et al.* (2005) developed a MRI-guided biopsy device and Susil *et al.* (2006) developed a device for MRI-guided transrectal biopsy, brachytherapy (HDR) and the implantation of fiducial gold markers. Both groups showed the feasibility of the devices, but randomised trials to compare treatment outcome with current techniques, are not available yet. At our department we are currently also working on the development of a robotic device for MRI-guided brachytherapy (Lagerburg *et al.*, 2006a). With this device we want to accurately place the iodine seeds to improve the dose distribution in the prostate. In literature some research regarding seed placement accuracy is described. Kaplan *et al.* (2004) describe in their study the precision of seeds deposited as loose seeds versus suture embedded seeds. They found a mean radial deviation of 3.1 mm with loose seeds and 3.7 mm with suture embedded seeds. Roberson *et al.* (1997) found a source placement error relative to the pre-planned position of 4.6 ± 1.8 mm and Taschereau *et al.* (2000) found a seed displacement of 6.1 mm with locking needles and 6.3 mm without locking needles. Deviations from the pre-planned position may influence the dose distribution in the prostate significantly (Dawson *et al.*, 1994; Moerland *et al.*, 1997). Dawson *et al* showed in a simulation study that with a maximum error in the placement of each seed of 2 mm an overdose of 12 % relative to the planned dose distribution is possible. Because of the better image quality of MRI compared to ultrasound and the possibility of accurate positioning with a robotic device we expect higher seed placement accuracy with our robotic device.

Although MRI has advantages for prostate brachytherapy, there are also some difficulties. The two major difficulties in MRI-guided procedures are the limited space inside the closed bore and the forces and torques of the magnetic field on surgical instruments. This makes it necessary to adapt the currently used methods and materials for prostate interventions. Robotics make it possible to perform the interventions inside the small space of the closed bore, but attention has to be paid to the materials used. Even when non-magnetic materials are used during the procedure, the image can be distorted by susceptibility artifacts, which undo the advantage of the good image quality of MRI. Therefore

materials with a susceptibility close to that of human tissue, such as plastics and ceramics, should be used as much as possible.

1.4   Robotics in prostate cancer

Robotic devices might be very useful in the detection and treatment of prostate cancer, because of their potential for improving the precision and capabilities of the physician to perform surgical procedures. In prostate brachytherapy another advantage is the potential reduction of manual handling of seeds and concomitant radiation exposure.

In the detection of prostate cancer robotics can be valuable in performing the biopsy procedure. Engelhard *et al.* (2006) and Beyersdorff *et al.* (2005) both developed a device for MRI-guided prostate biopsy. Beyersdorff *et al* developed a device made of polyoxymethylene that consists of a base plate, an adjustable arm, and a needle guide. The needle guide can be manipulated from outside the MRI unit by means of a telescopic rod. The needle guide is filled with contrast material gel that can be visualised at MR imaging. Biopsy was performed with transrectal access and with the patients in prone position. They claim that in most cases imaging is not required during needle deployment, because the needle guide of the biopsy device has a defined length and is used with a needle of constant length. Engelhard *et al* performed the biopsy in supine position. They used a biopsy device that was composed of a ground plate, which was fixed to the table extension. On top of it a guiding device was placed which could be mechanically angled by hand in three directions. At the end of the guiding device a needle guide, filled with contrast agent was inserted, which was used as a guide rail for the biopsy needle. They imaged, in contrast to Beyersdorff, the needle in the target lesion to prove the correct needle position in the suspicious area. In this way the needle position can be corrected for subtle changes in patients and prostate position. Both groups showed the easibility of the robotic device in a patient study.

For prostate resection different robotic systems are in use. The Imperial College in London e.g. uses a robotic system named Probot to aid in transurethral resection of the prostate, while the University of Chicago Pritzker School of Medicine uses the three-arm da Vinci Robotic System (Harris *et al.*, 1997; Mikhail *et al.*,

2006). Robot-assisted laparoscopic prostatectomy offers advantages compared to the straight laparoscopic technique, such as increased freedom of maneuverability, and filtered tremor. Disadvantages are e.g. the loss of tactile sensation and the high cost of purchase and maintenance.

Several research groups are working on the development of a robotic device for prostate brachytherapy. They can be separated in two different categories. One that is mainly focussing on the advantages of robotics in replacing the physician and one that is focussing on image quality during the procedure. Especially when one wants to perform MRI-guided brachytherapy in a closed bore scanner, which gives a better image quality than an open scanner, a robotic device is needed, because of the limited space inside the scanner.

Fichtinger *et al.* (2006) designed a robotic device for transperineal ultrasound-guided prostate brachytherapy. It consists of a needle placement robot which is spatially registered to the ultrasound probe. The working of the device was tested on a phantom. The concept and technical feasibility of the robotic device was shown, but major redesign of the robot hardware and needle/seed tracking modules is in progress to improve the performance. A disadvantage of the system is that it makes use of preloaded needles. After the seed is implanted and the needle retracted, the empty needle has to be removed and replaced with the next preloaded needle. Yu *et al.* (2006) developed a 16 DOF (Degrees-Of-Freedom) robotic system for ultrasound-guided prostate brachytherapy as well. The main objectives of this robotic device were: increase of accuracy of needle placement and seed delivery, reduction of trauma and oedema, reduction of radiation exposure, shorter learning curve and a reduced OR (Operating Room) time. Some preclinical experiments showed the feasibility of the device. Clinical experiments still have to be performed. Schneider *et al.* (2004) developed a robotic system for transrectal needle insertion into the prostate with integrated ultrasound. The main goal of this system is to provide accurate and predictable transrectal needle placement. The system makes use of a curved needle guide along the ultrasound probe. Phantom experiments showed accurate needle placement.

Fichtinger *et al.* (2002a) designed a device for robotically assisted prostate biopsy and therapy with intraoperative CT guidance. This device inserts the needle under an arbitrary angle anywhere in the prostate. This technique overcomes the problem of pubic arch interference encountered in the parallel needle

insertion technique. In comparison with transrectal US, CT has two obvious shortcomings, its lack of true real-time imaging and the toxic radiation that it delivers to the patient. Use of CT is advantageous for the localisation of implanted needles and seeds which makes it possible to update dosimetry intraoperatively. Pre-clinical experiments suggested that the primary cause of needle-placement error is needle-tissue interaction. To compensate for displacement of the prostate gland they intend to use bilateral stabilisation needles. Further experiments are needed to evaluate the accuracy and safety of the system.

Muntener *et al.* (2006) and Patriciu *et al.* (2007) describe the development and some preclinical experiments of a MRI compatible robot capable of automated brachytherapy seed placement. A new type of pneumatic actuator was specifically developed for this application. Fiducial markers are attached to the end-effector and are used to register the robot in the MRI scanner. The end-effector can easily be replaced with an other end-effector for e.g. biopsy. The results of the first tests in phantoms are promising, with a seed placement accuracy of 0.72 ± 0.36 mm. Before any clinical use more extensive testing is necessary. Fichtinger *et al.* (2002b) and Susil *et al.* (2003, 2004, 2006) describe the development of a robotic device that is suitable for several prostate interventions. They first describe the development of a prototype robotic device for transrectal needle insertion. This device consists of an end-effector that is introduced into the patient's rectum, a motion stage to provide translation and rotation for the end-effector, an insertion stage to enter the needle into the prostate and retract it, an adjustable mount to bring and secure the device in optimal initial position, and actuation shafts for remote operation from outside the scanner. After some preclinical tests, this device was successfully tested on canines which were placed in a prone position (Susil *et al.*, 2003).

Susil *et al.* (2004) describe the development of a system for biopsy and High Dose Rate (HDR) prostate brachytherapy. This system is capable of planning and execution of transperineal needle insertion and consists of a lockable positioning arm, an endorectal imaging coil and a custom-built perineal template. The patient is placed in the left lateral decubitus position to maximise perineal exposure. After biopsy sites were selected, the patient table was withdrawn from the scanner to insert the biopsy needles. The patient was then advanced back into the scanner and, prior to tissue collection, images were acquired to

verify placement of the needle. Following biopsy collection, needle insertion for HDR brachytherapy was performed. For the HDR treatment the patient was subsequently transferred to a shielded room for radiation delivery. A major concern with the left lateral decubitus position for a prolonged period is the stability of the position and the potential for brachial plexopathy and injuries to cutaneous pressure points.

At our own department we are currently working on the development of a Single Needle Implant Device (SNID) for MRI-guided prostate brachytherapy (Van Gellekom *et al.*, 2004). With this device the needle is tapped into the prostate, instead of the currently used method of pushing, to diminish prostate motion during needle insertion. A new implantation method, the single needle implant method was designed, because of the limited space inside the closed bore MRI scanner. With this method, only one needle is used, which is inserted through a rotation point, close behind the skin. After the seed is placed, the needle is retracted to the rotation point and re-inserted at a different angle. This method makes it possible that the patient stays in the MRI scanner during the whole procedure. In Figure 1.1 pictures of the various robotic devices for MRI-guided brachytherapy are shown.
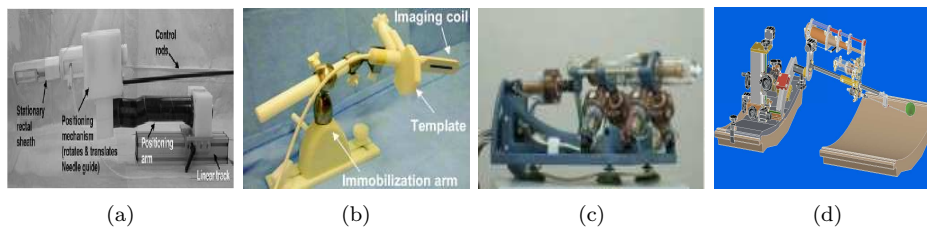

(a)   (b)   (c)   (d)

Figure 1.1: Pictures of a (a) robotic device for transrectal prostate brachytherapy (Susil *et al.*, 2003) (b) system for transperineal HDR prostate brachytherapy (Susil *et al.*, 2004) (c) robotic device for transperineal prostate brachytherapy (Muntener *et al.*, 2006) (d) robotic device for prostate brachytherapy from our own department

1.5 Outline

In this thesis the first steps in the development of a robotic device for MRI-guided prostate brachytherapy are described. In chapter 2 prostate rotation during needle insertion is investigated. This is done because the robotic device will use a different implantation technique (single needle implant method (Van Gellekom *et al.*, 2004)), which makes prostate motion during needle insertion more important. With the currently used method first all needles are inserted, before the seeds are delivered. The prostate is more or less fixated and prostate motion will be minimal. With the new method one needle is used. This needle is inserted into the prostate, a seed is delivered, the needle is retracted, re-inserted under a different angle and the next seed is delivered. With this method prostate motion is possible with each needle insertion, which might influence the seed positions. In chapter 3 the first step in the development of the robotic device is described. A prototype tapping device is developed, which should minimise prostate motion during needle insertion. The clinical validation of the tapping device is described in chapter 4, where two groups of patients are compared for their prostate motion during needle insertion. In the first group the commonly used method of manually pushing the needle into the prostate is used and in the second group the needles are tapped into the prostate with a prototype robotic device. In chapter 5 the artefact of an Iodine seed placed at the needle tip was simulated. The influence of different needle materials on this artefact was analysed. To validate the simulations some of them were compared with real MRI experiments. Finally, in chapter 6 the design of the first prototype of the robotic device is described. Some first MRI compatibility tests were performed to test the working of the device in a magnetic field.

Chapter 2

Measurement of prostate rotation during insertion of needles for brachytherapy

Abstract

Purpose: The purpose of this study is to investigate whether prostate rotation due to needle insertion for prostate brachytherapy is predictable and if so, to quantify this rotation, and to see whether locking needles reduce the magnitude of prostate rotation.

Methods and Materials: The measurements are done at the beginning of the procedure for brachytherapy with a Foley catheter in situ. After a needle is inserted into the prostate, a 3D ultrasound scan is made. Then the seeds are delivered using RAPID Strands (Oncura), and the needle is withdrawn. A second 3D scan is made. The needle and seed positions are determined in these scans. To determine the rotation of the prostate, the angle between the needle and the seed trajectory is calculated.

Results: The prostate rotations have been measured in sixteen patients, eight without the use of locking needles and eight with locking needles. In total 62 needles were inserted. The maximum rotation was 13.8 degrees and occurred in the coronal plane when no locking needles were used with a significant correlation ($p < 0.01$, $R = 0.637$) between the place of insertion and rotation. It was shown that the method (with or without locking needles) had a significant ($p < 0.001$) influence on the rotation

in the coronal plane. Rotations in the sagittal plane ranged from -8.5 degrees to +10.2 degrees without correlation with the insertion point of the needle or the use of locking needles.

Conclusion: This study showed that prostate rotation during needle insertion for prostate brachytherapy is relatively large and unpredictable. Locking needles reduce prostate rotation in the coronal plane, but not in the sagittal plane. Minimising this rotation is necessary for accurate seed delivery, especially when a robotic implantation technique is used.

2.1   Introduction

In brachytherapy of prostate tumours it is possible to deliver an adequate radiation dose to the prostate while sparing critical surrounding organs like the urethra, the neurovascular bundles, and the rectum (Merrick *et al.*, 2001; Stone and Stock, 2002; Merrick *et al.*, 2003b,a). Source placement precision is an important limiting factor for the optimisation of the dose distribution, since deviations from pre-planned positions may effect the planned dose significantly (Dawson *et al.*, 1994; Moerland *et al.*, 1997). The insertion of needles for seed delivery in prostate brachytherapy is currently done under ultrasound guidance (Holm *et al.*, 1983). Disadvantages of ultrasound-guided brachytherapy are the poor visibility of the prostate, especially at the base plane and the apex, which makes it difficult to estimate the prostate volume, and the difficulty to visualise the implanted Iodine seeds, hence intra-operative dose calculation is based on needle positions rather than seeds positions (Van Gellekom *et al.*, 2004).

Compared with ultrasound, Magnetic Resonance Imaging (MRI) offers a better soft tissue contrast, which gives it the potential for better delineation of the prostate capsule and for definition of structures inside the prostate (Cheng and Tempany, 1998; Husband *et al.*, 1998; Rasch *et al.*, 1999). This makes it possible to further optimise the dose distribution by giving certain parts of the prostate a different dose.

Because of the limited space inside a closed bore MRI scanner and the risk of pubic arch interference, current template guided transperineal implant techniques have their limitations. The development of a single needle implant device, that can be placed between the legs of a patient in a MRI scanner, can

overcome these problems (Van Gellekom *et al.*, 2004). This robotic system will insert one needle under different angles into the prostate to deliver the seeds. After delivering the seeds, the needle will be retracted to the rotation point just beneath the skin and the insertion angle can be changed. The procedure will be performed without the use of a template or locking needles (Figure 2.1(a) and 2.1(b)). With this method it is not necessary to move the patient in and out the MRI scanner during the procedure, as with other MRI-guided prostate intervention methods (Ménard *et al.*, 2004; Susil *et al.*, 2004).

(a) (b)
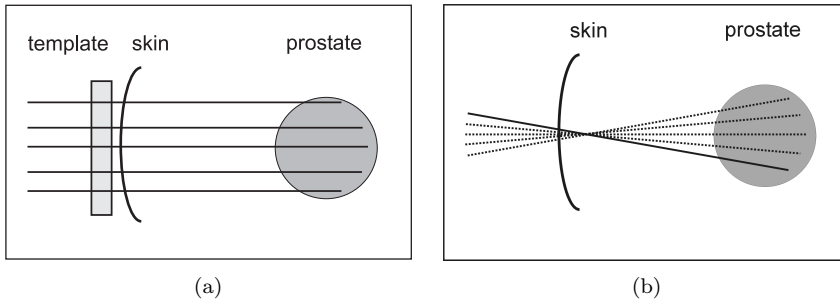
Figure 2.1: Schematic visualisation of (a) the multi parallel needle method and (b) the single needle method.

The single needle implant method is a needle by needle method, whereas in the current template guided method firstly all needles are placed before seed delivery. This means that, except for the first few needles, the prostate is fixated. Using the single needle method, the prostate can rotate with every new insertion of the needle. Prostate motion (rotation and displacement) and needle divergence are known causes of source misplacement (Roberson *et al.*, 1997; Nath *et al.*, 2000). Due to needle insertion the prostate position and shape will change during the procedure. This makes it difficult to deliver the seeds to the desired (pre-planned) position. Besides for prostate brachytherapy, tissue movement can also be a problem in taking biopsies, e.g. in breast biopsies (Deurloo *et al.*, 2001).

Feygelman *et al.* (1996) and Dattoli and Waller (1997) suggest that locking needles can help stabilise the prostate to reduce seed misplacement, while Taschereau *et al.* (2000) found no effect of locking needles. Even if locking needles reduce the prostate motion, it is necessary to be able to predict the changes in prostate position and shape to be able to deliver the seeds at the

desired position.

The purpose of this study is to investigate whether prostate rotation due to needle insertion for prostate brachytherapy is predictable and if so, to quantify this rotation, and to see whether locking needles reduce the magnitude of prostate rotation.

2.2   Methods and Materials

2.2.1 Implant procedure

The current implant procedure in our institute is performed with patients placed in lithotomy position (Battermann, 2000). A Foley catheter is placed before the introduction of the needles. A rectangular template with 5mm spaced holes is positioned against the perineum. Two locking needles are inserted into the prostate, one on each side. Thereafter the needles are inserted parallel to each other and are used for the delivery of the Iodine seeds. Before the seeds are delivered, the position of the needles in the prostate is verified and adjusted if necessary. At our institute two techniques of delivering the seeds are applied, viz. manually using RAPID Strands (Oncura, Eindhoven, The Netherlands) or automatically using single selectSeeds and the FIRST System (Nucletron, Veenendaal, The Netherlands). The whole procedure is performed under ultrasound guidance.

2.2.2 Measurements

For our study the normal procedure was changed slightly for the first few inserted needles. Instead of first inserting all needles and then delivering the seeds, the procedure was performed needle per needle. Doing so the rotation of the prostate is not influenced by the presence of other needles and this simulates the situation we will have when we use the single needle implant method. The seeds are delivered manually using RAPID Strands, because of two reasons. Firstly with RAPID Strands the seeds are positioned more or less in a straight line, which makes it more easy to determine the prostate rotation. Secondly with this procedure it is more easy to deliver the seeds needle per needle.

The prostate rotations have been measured in sixteen patients, eight without locking needles and eight with locking needles in situ. Only the first three or four needles per patient were used for our measurements (mean number of total inserted needles per patient was 27; range 20 - 37). After these needles the normal procedure went on. In total 62 needles were analysed, 31 needles without locking needles in situ and 31 with locking needles in situ. The measurements were done at the beginning of the procedure for brachytherapy with the Foley catheter in situ. After a needle was inserted into the prostate, a 3D ultrasound scan was made. Then the strand with seeds was delivered, and the needle was withdrawn. A second 3D scan was made. The needle and seed positions were determined in these scans. This was done twice, on different moments (the time between those moments varied from 6 to 114 days; mean 30 days; median 16 days), by the same observer, to verify the reproducibility of the measurements. To determine the rotation of the prostate, the angle between the needle and the seed trajectory was calculated (see Figure 2.2) in the coronal plane and in the sagittal plane to get the rotations around the anterior-posterior (AP) axis and the left-right (LR) axis, respectively. The centre of the prostate was also defined. This was done because we expected to find a correlation between the place of insertion of the needle (calculated as the distance between the centre of the prostate and the insertion point) and the rotation of the prostate. Per patient a needle was inserted in every quadrant of the prostate.

2.2.3 Statistics

The calculated rotations were analysed using SPSS and Scilab. Firstly the correlation between the place of insertion and the rotation was calculated. After this the differences in prostate rotation between the two methods (with or without locking needles) were analysed. Regression analysis was used for this, with the rotation as dependent factor, the method as fixed factor and the distance of the insertion point from the centre of the prostate as covariate. Because the predicted residues were not normally distributed standard parametric tests were not appropriate. Instead, we made use of bootstrapping. Bootstrap is a resampling technique in which the elements of the original sample are used as if they represent the whole studied population. A bootstrap sample $x^* = (x_1^*, x_2^*, ... , x_n^*)$ is obtained by randomly sampling n times, with replacement, from the original data points x_1, x_2, ..., x_n (Efron and Tibshirani, 1993). This

(a)   (b)
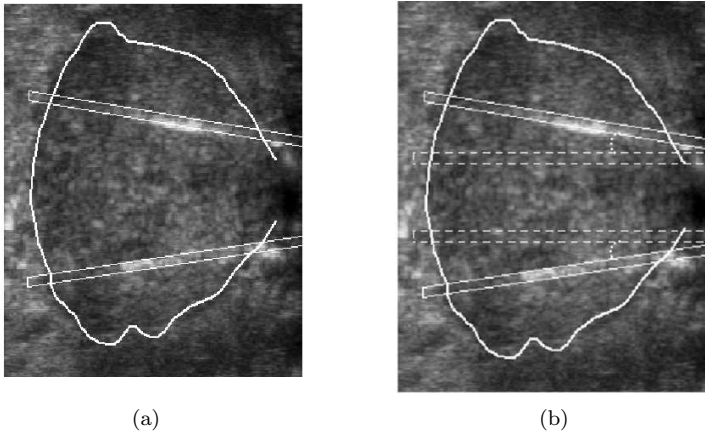
Figure 2.2: Example of (a) an ultrasound scan with the seed trajectories and (b) how the angles are calculated. The dashed lines depict the needles, the solid lines are the seed trajectories, and the dotted lines indicate the angle between those two.

was done a large number of times and the statistics we were interested in were performed on every sample. The computed values for the statistics form an estimate of the sampling distribution of the statistic.

2.3   Results

Before analysing the results we checked the reproducibility of the measurements. All the data was checked twice (on different times) and there were no significant differences found between these measurements. The mean difference $\pm$ the standard deviation for the insertion point in the coronal plane was 0.19 ± 0.96 mm and in the sagittal plane -0.03 ± 0.63 mm. The mean difference for the rotation in the coronal plane was -0.42 ± 2.83 degrees and -0.13 ± 1.53 degrees in the sagittal plane. Furthermore we checked if the places of insertion for the needles were the same for both methods (with and without locking needles). No significant differences were found.

The range, minimum and maximum of the measurements are presented in Table 2.1. The rotation of the prostate is defined as negative when the seeds at the base plane are located more to the right/anterior than the needle. The largest

rotation in the coronal plane was 13.8 degrees without locking needles (ϕ_{cor1}) and -7.8 with locking needles (ϕ_{cor2}). In the sagittal plane the largest rotation was -8.5 degrees without locking needles (ϕ_{sag1}) and 10.2 degrees with locking needles (ϕ_{sag2}). The rotation of the prostate results in a deviation between the real seed position and the planned seed position. With a prostate rotation of 13.8 degrees and a strand existing of four seeds the maximum displacement of the seeds relative to the planned position that can occur is 8.4 mm. The variances for the rotation in the coronal plane differ significantly (p = 0.01) for both methods, which means that the spread was much larger in one of the two methods. This corresponds with a difference in ranges for the prostate rotation for both methods; for method 1 (without locking needles) the range is 25.0 degrees and for method 2 (with locking needles) the range is 12.0 degrees. In the sagittal plane no significant difference in the range of the rotation for both methods was found. For the rotation in the coronal plane, without locking needles, there was a correlation found with the place of insertion (x_1) of 0.637 (p < 0.01). With locking needles (x_2) there was no significant correlation (p = 0.902) in the coronal plane. In the sagittal plane there was no significant correlation found for both methods.

	range	minimum	maximum
x_1	37.8	-18.2	19.6
ϕ_{cor1}	25.0	-11.2	13.8
x_2	41.4	-22.2	19.3
ϕ_{cor2}	12.0	-7.8	4.2
y_1	30.3	-11.0	19.3
ϕ_{sag1}	16.2	-8.5	7.7
y_2	30.2	-14.5	15.6
ϕ_{sag2}	11.9	-1.7	10.2

Table 2.1: Range, minimum and maximum of the variables (distance between insertion point and centre of the prostate for both methods (without (1) and with (2) locking needles), in the coronal plane (x) and the sagittal (y) plane and the prostate rotation (ϕ) for both methods in both directions).

In Figure 2.3 the data of our measurements are shown. It was found that the method (with or without locking needles) had a significant (p < 0.001) influence on the rotation in the coronal plane; which means that the regression lines for the two methods differ significantly:

Method 1: ϕ_{cor} = -0.42 + 0.26 * x

Method 2: ϕ_{cor} = -0.86 + 0.00 * x

In the sagittal plane no significant difference was found between the two methods (p = 0.7).
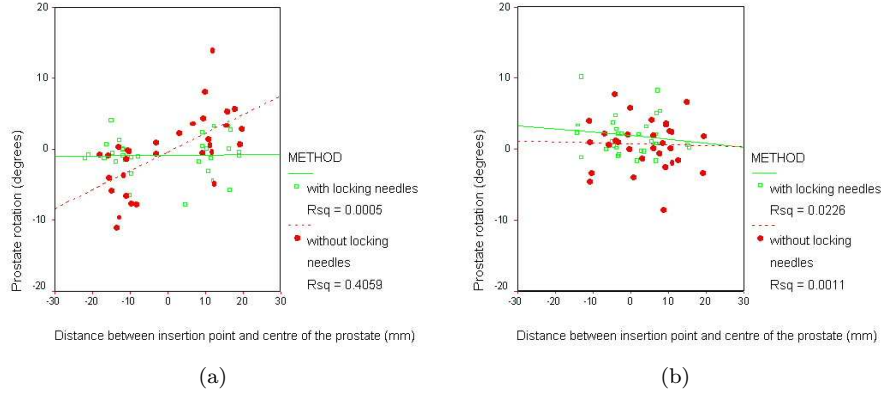
Figure 2.3: Distance of the insertion point of the needle from the centre of the prostate (x or y) against the rotation of the prostate (ϕ_{cor} or ϕ_{sag}) for both methods (without locking needles and with locking needles) in the (a) coronal plane and (b) sagittal plane.

2.4   Conclusion and Discussion

To our knowledge only little is known about prostate rotation due to needle insertion. Displacement and deformation of the prostate during needle insertion were subject of several theoretical and simulation studies (DiMaio and Salcudean, 2002b; Alterovitz *et al.*, 2003b,a; DiMaio and Salcudean, 2002a), but measured data are scarce (Stone *et al.*, 2002). Taschereau *et al.* (2000) studied the effect of stabilising needles on accuracy of needle insertion and found no benefit. The insertion angle of the needle relative to the insertion axis was measured, from which, however, the prostate rotation can not be derived.

The results of our study show that prostate rotation during needle insertion is relatively large. Before starting the experiments we expected the rotation of the

prostate to correlate with the place of insertion of the needles. It was shown that this expectation is only correct for the coronal plane when no locking needles are used. This means that in this situation we are able to predict the rotation of the prostate with a certain reliability ($R^2 = 0.41$), with the help of its regression line.

The rotation of the prostate in the coronal plane is influenced by the use of locking needles. The prostate still rotates when locking needles are used, but the rotation becomes significantly less. This agrees with the conclusion found in literature that locking needles can help stabilise the prostate during prostate brachytherapy. Dattoli and Waller (1997) found a decrease of the maximum lateral displacement from about 1 cm to 0.2 mm when locking needles were used. Feygelman *et al.* (1996) compared the use of two and three locking needles which each other and found a better target volume coverage (V_{100}) when three locking needles were used (94% against 85%). Taschereau *et al.* (2000) found only small effects of the use of locking needles, the mean insertion angle e.g. decreased from 6.6 to 6.2 degrees when locking needles were used. In these studies all needles were inserted into the prostate before evaluation of the influence of locking needles.

In our study, the rotation of the prostate in the sagittal plane was not reduced by the use of locking needles.

In the coronal plane, when no locking needles are used, the prostate is relatively free to rotate. In this direction the rotation correlates well with the distance between the prostate centre and the insertion point. The use of locking needles prevents the prostate to rotate freely.

Because, especially in the sagittal plane, the prostate rotation is more or less random, even if locking needles are used, it is very difficult to take this rotation into account when inserting the needle. One approach to solve this problem may be the use of markers in the prostate that can be visualised in ultrasound or eventually MRI so that prostate rotation during needle insertion can be depicted. Markers are already used in some institutes to quantify the motion of the prostate during radiotherapy (Balter *et al.*, 1995a; Crook *et al.*, 1995; Dehnad *et al.*, 2003). A second approach is to develop a method of needle insertion that avoids prostate rotation and deformation. This approach will be the subject of the next step in this study, where we will measure the prostate rotation when tapping the needle into the prostate instead of pushing, because

we expect the prostate rotation being less with this method.

In conclusion, prostate rotation occurred in the coronal plane and in the sagittal plane of the prostate, resulting in seed depositions that differ several mm from their planned positions. Only rotation in the coronal plane can be more or less predicted and reduced by the use of locking needles. Rotation in the sagittal plane can not be predicted. Other needle insertion techniques are under investigation to reduce prostate rotations and thus to increase seed deposition accuracy.

Chapter 3

Development of a tapping device: a new needle insertion method for prostate brachytherapy

Abstract The purpose of this study is to develop and test a tapping device for needle insertion for prostate brachytherapy. This device will tap the needle into the prostate with a certain, well-defined, amount of momentum, instead of the currently used method of pushing the needle. Because of the high needle insertion velocity, we expect prostate motion and deformation being less compared to current methods.

We measured the momentum that is applied when manually tapping the needle into the prostate and found a mean momentum of 0.50 ± 0.07 Ns. The tapping device is pneumatically driven and we found that the delivered momentum increased linearly with the applied air pressure. The efficacy of the tapping device was tested on a piece of beef, placed on a freely moving and rotating platform.

A significant correlation was found between the applied pressure and the rotation and displacement of the beef. Displacements and rotations were minimal for the highest

pressure (4 bar) and amounted only 2 mm and 6 degrees, respectively. Higher air pressures will further reduce displacements and rotations.

3.1   Introduction

Brachytherapy is one of the treatment possibilities for early stage prostate cancer. With brachytherapy it is possible to deliver an adequate radiation dose to the prostate while sparing critical structures like the urethra, the neurovascular bundles, and the rectum (Merrick *et al.* (2001); Stone and Stock (2002); Merrick *et al.* (2003b,a)). One of the limiting factors of dose optimisation in prostate brachytherapy is source placement precision. Seed positions that deviate from the pre-planned positions may influence the dose distribution in the prostate significantly (Dawson *et al.* (1994); Moerland *et al.* (1997)).

The insertion of needles for prostate brachytherapy is currently done under ultrasound-guidance (Holm *et al.* (1983)). Disadvantages of ultrasound-guided brachytherapy are the poor visibility of the prostate, especially at the base plane and the apex, which makes it difficult to estimate the prostate volume, and the difficulty to visualise the implanted Iodine seeds, hence intra-operative dose calculation is based on needle positions rather than seeds positions (Van Gellekom *et al.* (2004)).

Compared with ultrasound, Magnetic Resonance Imaging (MRI) offers a better soft tissue contrast, which gives it the potential for better delineation of the prostate capsule and for definition of structures inside the prostate (Cheng and Tempany (1998); Husband *et al.* (1998); Rasch *et al.* (1999)). This makes it possible to further optimise the dose distribution e.g by dose reduction in the penile bulb to reduce the risk of impotence (Merrick *et al.* (2002)) or by dose increase to the intraprostatic lesion to improve biochemical, disease-free survival (De Meerleer *et al.* (2005)).

Because of the limited space inside a closed bore MRI scanner and the risk of pubic arch interference, current template guided transperineal implant techniques have their limitations (Ménard *et al.* (2004); Susil *et al.* (2004)). The development of a single needle implant device, that can be placed between the legs of a patient in a MRI scanner, can overcome these problems (Van Gellekom *et al.* (2004)). This robotic system will insert one needle under different angles

into the prostate to deliver the seeds. After delivering the seeds, the needle will be retracted to the rotation point just beneath the skin and the insertion angle can be changed. The procedure will be performed without the use of a template or locking needles (Figure 3.1(a) and 3.1(b)). With this method it is not necessary to move the patient in and out the MRI scanner during the procedure, as with other MRI-guided prostate intervention methods (Ménard *et al.* (2004); Susil *et al.* (2004)).

(a) (b)
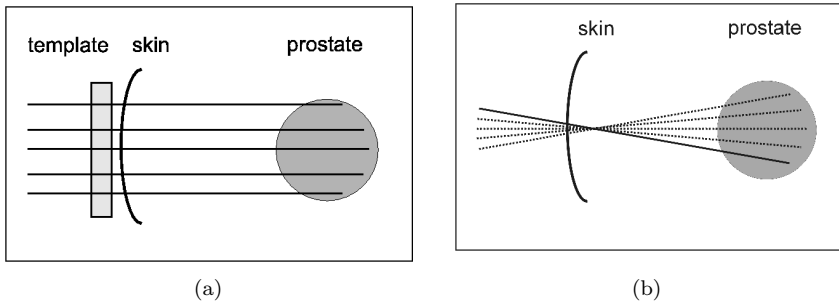
Figure 3.1: Schematic visualisation of (a) the multi parallel needle method and (b) the single needle method

The single needle implant method is a needle by needle method, whereas in the current template guided method firstly all needles are placed before seed delivery. This means that, except for the first few needles, the prostate is fixated. Using the single needle method, the prostate can rotate with every new insertion of the needle.

Feygelman *et al.* (1996) and Dattoli and Waller (1997) suggest that locking needles can help stabilise the prostate to reduce seed misplacement, while Taschereau *et al.* (2000) found no effect of locking needles. Even if locking needles reduce the prostate motion, it is necessary to be able to predict the changes in prostate position and shape to be able to deliver the seeds at the desired position.

In our own study (Lagerburg *et al.*, 2005) we found that only rotation in the coronal plane can be more or less predicted and reduced by the use of locking needles. Rotation in the sagittal plane can not be predicted nor reduced by the use of locking needles. The maximum rotation we found in the coronal plane was 13.8 degrees without locking needles and 7.8 degrees with locking needles.

In the sagittal plane the maximum rotation was 8.5 degrees without locking needles and 10.2 degrees with locking needles. The rotation of the prostate results in a deviation between the real seed position and the planned seed position. With a prostate rotation of 13.8 degrees and a strand existing of four seeds the maximum displacement of the seeds relative to the planned position that can occur is 8.4 mm

Prostate motion (rotation and displacement) and needle divergence are known causes of source misplacement (Roberson *et al.*, 1997; Nath *et al.*, 2000). Needles for prostate brachytherapy are currently pushed into the prostate by the physician. Due to the elastic properties of the prostate this results in movement and deformation of the prostate. This makes it difficult to deliver the seeds to the desired (pre-planned) position.

In this study we introduce a new needle insertion method to decrease prostate movement and deformation. Instead of pushing, the needle is tapped into the prostate. Due to the high needle insertion velocity, we expect the prostate to move less. We have made a device for needle insertion with a controlled velocity. The device will give a certain, well-defined, amount of momentum to the needle. With every tap the needle will be inserted at most a certain, beforehand defined, distance (e.g. 5 mm) into the prostate. This tapping device is the first part of the single needle implant device (SNID) (Van Gellekom *et al.*, 2004), which will be developed at our department and used for MRI-guided brachytherapy.

Besides for prostate brachytherapy this new needle insertion method can also be useful for other applications where tissue movement due to needle insertion is problematic such as e.g. breast biopsies (Deurloo *et al.*, 2001).

The purpose of this study is to measure the momentum that is necessary to insert a needle into the prostate and to develop and test a device that taps a needle into the prostate with a certain, well-defined, amount of momentum.

3.2   Methods and Materials

To develop a device that taps a needle into the prostate it is necessary to know the minimum momentum that is needed to insert a needle into the prostate. This momentum was measured during the normal procedure for prostate brachytherapy. The needle was tapped into the prostate by a physician (JJB). The

momentum was measured with a Flexiforce A201 sensor from Tekscan. The momentum that can be delivered by the tapping device is adjustable by changing the air pressure of the pneumatic cylinder. The working of the tapping device was tested on a piece of beef. Beef displacement and rotation were measured for different air pressures.

3.2.1 Calibration of the Flexiforce sensor

The Flexiforce A201 sensor is a flexible, thin film force sensor. The application of force to the sensor results in a change of the resistance of the sensing element, which is inversely proportional to the force applied. The sensor is suitable for measuring both static and dynamic forces. The sensor has to be calibrated to be able to convert the output into the appropriate engineering units.

The experimental setup to calibrate the Flexiforce sensor consisted of a pendulum and a hammer (see Figure 3.2). The Flexiforce sensor was attached to the pendulum and the hammer was used to create a momentum p. The principle of the experimental setup is based on the law of conservation of angular momentum for a completely inelastic collision (equation 3.1).

$$R_{impact} m_h v_h = L_{tot,before} = L_{tot,after} = I_p \omega_p \tag{3.1}$$

where R_{impact} is the arm of the momentum (see also Figure 3.3), m_h is the mass of the hammer, v_h is the velocity of the hammer directly before impact, $L_{tot,before}$ is the total angular momentum before the impact, $L_{tot,after}$ is the total angular momentum after impact, I_p is the moment of inertia of the combination of the pendulum and the hammer, and ω_p is the angular velocity of the pendulum.

The hammer is released from a certain height. Depending on this height the hammer will have a certain velocity before it hits the Flexiforce sensor attached to the pendulum. Then the pendulum will start moving. The initial position of the hammer, the starting angle γ, was different for every measurement and the value of the Flexiforce sensor F_{flex} and the maximum angular velocity ω of the pendulum were measured. With these values and equations 3.3 and 3.4 it was possible to calibrate the sensor. With this experimental setup there where two possibilities to calibrate the sensor, viz. with the starting angle of the hammer
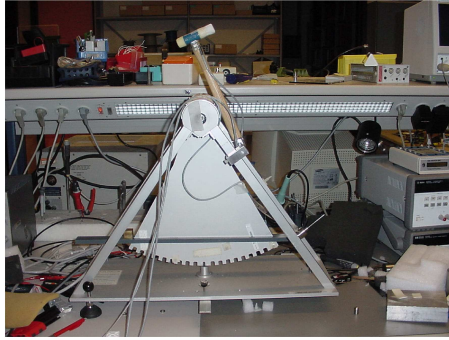
Figure 3.2: Experimental setup for the calibration of the Flexi-force sensor

(equation 3.4) and with the angular velocity of the pendulum after impact (equation 3.3). Both should give the same value for the conversion between the output of the Flexiforce sensor and the force.
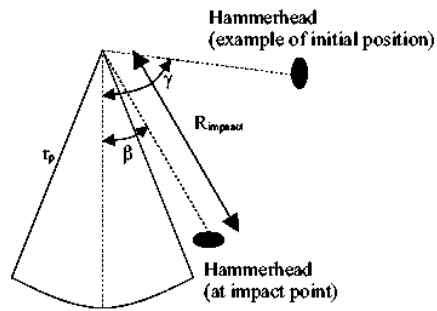

Figure 3.3: Schematic overview of the experimental calibration setup

The relationship between force and momentum is as follows:

$$\int_0^t F \; dt = mv = p \tag{3.2}$$

The value of the Flexiforce sensor is related to the angular velocity of the pendulum by:

$$\int_0^\tau F_{flex}\ dt = \frac{I_p \omega_p c}{R_{impact}} = \frac{m_p c r_p^2 \omega_p}{4\ R_{impact}} \tag{3.3}$$

where τ is the time duration of the impact process, F_{flex} is the output of the Flexiforce sensor, c is the conversion value between the output of the Flexiforce sensor and the force, and r_p is the radius of the pendulum.

The value of the Flexiforce sensor is related to the starting angle of the hammer by:

$$\int_0^\tau F_{flex}\ dt = m_h c \sqrt{2 g h_h (cos(\beta) - cos(\gamma))} \tag{3.4}$$

where g is the acceleration of gravity, h_h is the distance of the centre of mass with respect to the point of rotation of the hammer and β is the angle where the hammer hits the Flexiforce sensor (see also Figure 3.3).

3.2.2 Momentum measurements

The momentum measurements were performed during the procedure for prostate brachytherapy. The patient was placed in the lithotomy position and a Foley catheter was placed in situ. A rectangular template with 5mm spaced holes is positioned against the perineum. For our study the normal procedure was changed slightly for the first few inserted needles. Instead of pushing the needle into the prostate, the physician tapped the needle (18G) into the prostate using the same hammer that was used for the calibration measurements. The Flexiforce sensor was attached to the end of the needle. The output from the Flexiforce sensor was recorded after each tap, using an oscilloscope, and then transferred to a laptop. During the procedure the real-time ultrasound images of the prostate were recorded on video, on which we measured the distance that the needle was inserted into the prostate with every tap. This was measured because we expected a correlation between the used momentum and the distance that the needle was inserted into the prostate. The momentum measurements were performed in 2 patients. In total the insertion of 6 needles was analysed. After the insertion of the first few needles the normal procedure went on.

3.2.3 The tapping device

Figure 3.4 shows a schematic overview of the tapping device. The pneumatic cylinder used is a Festo ADVULQ-25-40-A-P-A-S20 (Delft, The Netherlands), with a maximum stroke of 40 mm. The pneumatic cylinder moves forward while pushing a sliding load. After the pneumatic cylinder reaches its maximum stroke the sliding load moves further with a constant velocity and hits the needle. The maximum insertion depth of the needle per tap is adjustable and a buffer stop is built in to prevent the insertion depth to exceed the previously defined distance. The maximum velocity of the pneumatic cylinder and thus the needle insertion velocity are adjustable by changing the air pressure.

The Flexiforce sensor was used to measure the momentum of the tapping device with different pressures (1 to 4 bar) and with two different sliding loads (33.2 gr and 121.6 gr). The tapping device should be able to deliver at least the same amount of momentum to the needle as the physician needed to insert a needle into the prostate.

The working of the tapping device was tested on a piece of beef. The beef was placed on a free rotating and movable platform (see Figure 3.5). The rotation (in the coronal plane) and translation (in the cranio-caudal direction) of the beef were measured for air pressures between 1 and 4 bar, after the needle was inserted 3, 4, 5 and 6 cm into the beef. The needle was inserted in the middle, 1 cm to the left and right and 2 cm to the left and right of the beef.
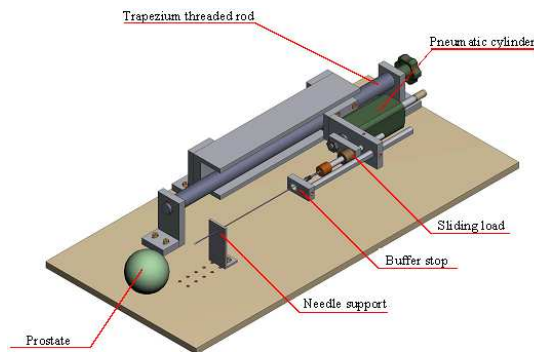
Figure 3.4: Schematic overview of the tapping device
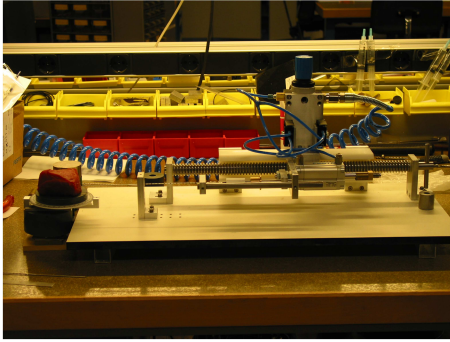
Figure 3.5: Experimental setup of the tapping device and the beef

3.3 Results

The calibration measurements were used to relate the values of the Flexiforce sensor found during the brachytherapy experiments and during the experiments with the tapping device to the force. There were two different conversion values found. With equation 3.3 a value for c of 107.4 ± 18 was found and with equation 3.4 a value for c of 73.2 ± 10.1 was found. There is a difference between these two values because after the collision the impulse from the hammer is not totally transferred to the pendulum. For this reason we used the value of 73.2 ± 10.1 for our further calculations. In Figure 3.6 an overview of the results is given.

During the brachytherapy procedure a mean of 3.7 taps per needle was necessary to insert the needle into the prostate. The needle was inserted between the 4.25 mm and 17.5 mm (mean 7.9 mm) into the prostate per tap. The momentum used to tap the needle into the prostate varied from 0.13 ± 0.02 Ns to 1.16 ± 0.15 Ns with a mean momentum of 0.50 ± 0.07 Ns. For the first tap there was a significant correlation $(R = 0.912, p = 0.011)$ between the momentum used and the distance that the needle was inserted into the prostate. There is also a significant correlation $(R = 0.620, p = 0.002)$ between the distance that the needle is already inserted into the prostate and the momentum needed to further insert the needle into the prostate. This means that for the first tap the relation between the momentum used and the distance that the needle was inserted into the prostate is different than for e.g. the third tap
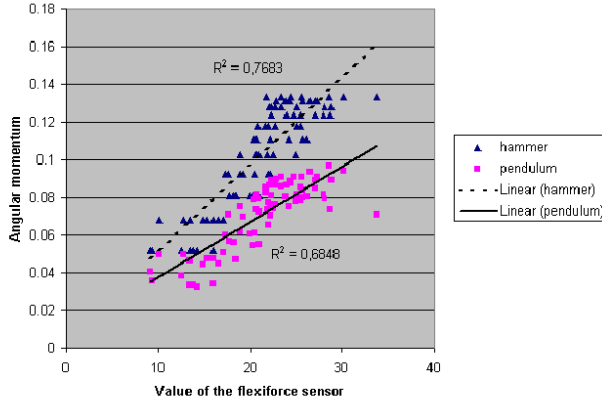
Figure 3.6: Relation between the value of the Flexiforce sensor and the angular momentum calculated with equation 3.3 for the pendulum and equation 3.4 for the hammer

$$tap1 : d = 0.29 * c * p \tag{3.5}$$

$$tap3 : d = 0.18 * c * p \tag{3.6}$$

where d is the distance that the needle is inserted into the prostate per tap in mm, c is the conversion value between the output of the Flexiforce sensor and the force and p is the momentum of the tap in Ns.

The momentum delivered by the tapping device depends on the used pressure and sliding load. The higher the pressure and the mass of the sliding load, the higher the achieved momentum. In Figure 3.7 the results of the measurements with the Flexiforce sensor in the tapping device are shown for the heaviest sliding load. When the sliding load of 121.6 grams and an air pressure of 4 bar is used the maximum momentum we can achieve is 0.37 ± 0.05 Ns. The insertion velocity of the needle depends on its weight. The needle insertion velocity we could reach during the experiment with the beef was 31 m/s.

The working of the automatic tapping device was tested on a piece of beef. An overview of the displacements and rotations of the beef for the two different sliding loads and the different air pressures is given in Table 3.1. It was shown that the displacement of the beef was significantly less for the most heavy load

(p = 0.002). For the rotation there was no significant difference found. Because we decided to use the most heavy load the rest of the results will be related to that load. There was a significant correlation found between the rotation of the beef and the place of insertion of the needle of 0.753 (p < 0.01). The correlation between the rotation and the pressure was -0.250 (p = 0.037). The displacement of the beef was correlated with the pressure and thus with the velocity of the pneumatic cylinder (R = -0.717; p < 0.01, see Figure 3.8). There was no correlation found between the displacement of the beef and the place of insertion of the needle. The maximum displacement found with a pressure of 4 bar was 2 mm and in all these cases the needle was inserted at least 4 cm into the beef. The maximum rotation found was 6 degrees and this was after the needle was inserted 5 cm into the beef.
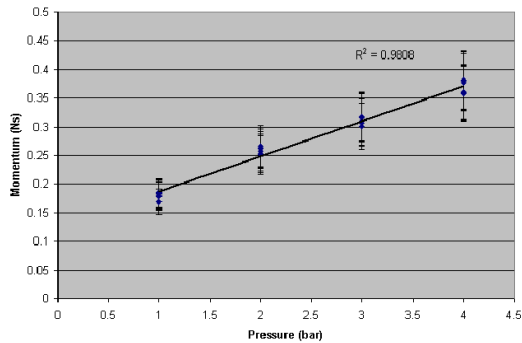
Figure 3.7: Relation between the air pressure and the momentum for the tapping device. The error bars give the standard deviation of the momentum.

3.4 Conclusion and Discussion

In this study a new method of needle insertion for prostate brachytherapy is described, viz. tapping the needle into the prostate instead of pushing. To be able to do this in a controlled and reproducible way a tapping device was developed. Before making this device the momentum needed to tap a needle into the prostate was measured during a normal brachytherapy procedure. The working of the tapping device was tested on a piece of beef.
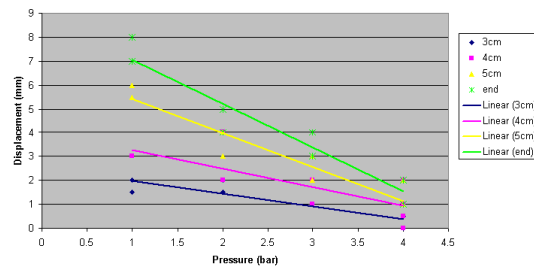
Figure 3.8: Relation between the air pressure and the displacement of the beef

Table 3.1: Minimum, maximum and mean rotations (absolute) and displacements of the beef for the two different sliding loads (33.1 gr and 161.2 gr) and different air pressures (1 to 4 bar). In the last column the maximum insertion depth of the needle into the beef is mentioned.

load	pressure		minimum	maximum	mean	in beef (maximum)
light	1	rotation (degrees)	2.0	6.0	3.6	4.1
		displacement (mm)	4.0	14.0	10.4	
light	2	rotation	0.0	9.0	3.2	6.0
		displacement	0.5	8.0	3.7	
light	3	rotation	0.0	6.5	1.9	6.3
		displacement	1.0	6.0	2.8	
light	4	rotation	0.0	10.0	2.8	6.3
		displacement	1.0	5.5	2.4	
heavy	1	rotation	0.0	16.0	4.3	5.7
		displacement	0.0	10.0	4.3	
heavy	2	rotation	0.0	9.0	3.5	6.4
		displacement	1.0	5.0	2.8	
heavy	3	rotation	1.0	6.0	3.3	6.2
		displacement	0.0	4.0	1.5	
heavy	4	rotation	0.0	6.0	1.3	7.1
		displacement	0.0	2.0	1.0	

Some research was already done to measure or model the forces during needle insertion (Holton, 2001; Kataoka *et al.*, 2002; Maurin *et al.*, 2004; Okamura *et al.*, 2004) and even a medical needle drive to investigate experimentally the mechanics of needle introduction in soft tissue already exists (Lefrançois and Sloboda, 2003). In our research we measured the momentum during needle insertion instead of the force. This is done because we made a device that taps a needle into the prostate with a high velocity and a certain, well-defined, amount of momentum, instead of the currently used method of pushing the needle. With this method we expect the prostate motion to be less. Furthermore, using momentum instead of force is safe to use. When the needle encounters e.g. a bony structure it will only transfer its momentum to the bony structure in a collision. It will not penetrate the bone as would happen when the needle was pushed into the prostate. The tapping robot will need a feedback system to detect incomplete needle insertion due to obstructions so that tapping is stopped under such circumstances.

During the calibration of the Flexiforce sensor we found two different constants for the conversion between the output of the sensor and the real force. The value we found with equation 3.3 for the pendulum was higher then the value we found with equation 3.4 for the hammer. This difference exists because the hammer does not transfer all its momentum to the pendulum after the collision, but it bounces back and continues moving. To prevent the hammer from bouncing back after the collision we attached a needle to the Flexiforce sensor and a piece of foam to the hammer, so the hammer will move together with the pendulum after the collision. With this method still not all the momentum from the hammer is transferred to the pendulum, but more than without the foam and the needle. The difference found between the momentum of the hammer and of the pendulum can be explained with a bouncing back of the hammer of 7 degrees (mean value), which corresponds with our observations during the experiments. Because of the above mentioned reason we used the conversion value calculated with equation 3.4 for further calculations. The value from equation 3.3 was only used as a reference value.

The spread in the conversion value can be due to three things; the hammer will not always hit the pendulum in exact the same way, which influences the value of the Flexiforce sensor, the movement of the hammer is not free of friction, which will also have its influence on the measurements and, the sensor also has

its own non-linearity.

During the brachytherapy experiments a correlation was found between the distance that the needle is already inserted into the prostate and the momentum needed to further insert the needle into the prostate. This indicates that there is friction between the needle and the prostate tissue. The correlation between the momentum used and the distance that the needle is inserted into the prostate decreases for every tap. This is probably also due to the friction between the needle and the prostate tissue. Because the needles are not inserted the same distance for each tap the influence of the friction differs for every tap.

With the tapping device it is possible to insert a needle into the prostate with different velocities. Before starting the experiments, we expected the prostate motion to correlate with the needle insertion velocity. This expectation was supported by the simulation studies of Alterovitz *et al.* (2003a) where they found that seed placement errors decrease with higher needle insertion velocities. During the beef experiments it was shown that this expectation is correct for the displacement and the rotation of the beef. The higher the velocity, the less displacement and rotation was found.

Displacement and deformation of the prostate during needle insertion were subject of several theoretical and simulation studies (DiMaio and Salcudean, 2002b; Alterovitz *et al.*, 2003b,a; DiMaio and Salcudean, 2002a), but measured data are scarce (Dattoli and Waller, 1997; Stone *et al.*, 2002). Dattoli and Waller (1997) found a displacement of the prostate of 1 cm without locking needles and 0.2 mm with the use of locking needles in the lateral direction. Stone *et al.* (2002) found maximum movement of the prostate in the cranial-caudal direction that ranged from 0 to 30 mm (median 15 mm). In the lateral plane a mean displacement of 1.93 and a maximum displacement of 4.61 mm was found. In the anterior-posterior plane a mean displacement of 2.60 mm and a maximum displacement of 5.86 mm was found. In our experiments with the beef we only tested for displacement along the cranio-caudal direction and a maximum displacement of 2 mm was found with an air pressure of 4 bar. This is significantly less than the displacement found in literature.

To our knowledge only little is known about prostate rotation due to needle insertion. In our own study we found that the maximum rotation in the coronal plane was 13.8 degrees and in the sagittal plane 8.5 degrees when no locking needles were used and the needles were pushed into the prostate (Lagerburg

et al., 2005). In our tapping experiments with the beef the rotation was only measured in the coronal plane and a maximum rotation of 6 degrees was found.

The next step in this study will be to test this device on patients to see whether the prostate movement and rotation really becomes less with this new needle insertion method. During these tests we also have to see if the momentum requires changes after several insertions due to decrease in sharpness of the needle.

In conclusion, an automatic tapping device was developed to insert a needle into the prostate for prostate brachytherapy. The experiments on beef showed that displacement and rotation due to tapping were less than found in literature when a needle was pushed into the prostate. From the brachytherapy experiments we can conclude that the optimal momentum of the tapping device may be somewhat higher then the now used 0.37 Ns, resulting in even less phantom movement.

Besides for prostate brachytherapy this new needle insertion method can also be useful for other applications where tissue movement due to needle insertion is problematic such as e.g. breast biopsies (Deurloo *et al.*, 2001).

Chapter 4

A new robotic needle insertion method to minimise attendant prostate motion

Abstract

Background and Purpose: The purpose of this study is to investigate the efficacy of a new needle insertion method (tapping instead of pushing) in reducing attendant tissue motion. This can be useful in applications where tissue motion due to needle insertion is problematic such as e.g. MRI-guided prostate brachytherapy and breast biopsies. In this study we will focus on prostate motion due to needle insertion.

Material and Methods: Prostate motion due to needle insertion was measured in 30 patients, who were transperineally implanted with fiducial gold markers for position verification in prostate intensity modulated radiotherapy. In total 32 needles were manually pushed into the prostate and 29 were tapped with a prototype robotic system. The prostate motion in the cranio-caudal direction was measured on the video record of the ultrasound images. Differences in prostate motion between the two needle insertion methods were analysed making use of SPSS.

Results: The mean prostate motion was 5.6 mm (range 0.3 - 21.6) when the needle was pushed and 0.9 mm (range 0 - 2.0) when the needle was tapped into the prostate ($p < 0.001$).

Conclusion: Prostate motion was significantly less when the needle was tapped into

the prostate compared to when the needle was pushed. This result is important for the development of a tapping, MRI-guided, prostate implant robotic system.

4.1   Introduction

Percutaneous needle insertion is a commonly used procedure in medical treatments. One of the difficulties during needle insertion is the precise placement of the needle. Due to needle insertion and retraction tissue movement will occur, which will limit the needle placement accuracy. In e.g. breast biopsy this will limit the diagnostic accuracy (Deurloo *et al.*, 2001) and in prostate brachytherapy tissue motion may result in seed positions that deviate from the pre-planned positions (Roberson *et al.*, 1997), which may influence the dose distribution in the prostate significantly (Dawson *et al.*, 1994; Moerland *et al.*, 1997). In this study we will focus on prostate movement due to needle insertion, but the results can also be useful for other applications such as e.g. breast biopsies.

Feygelman *et al.* (1996) and Dattoli and Waller (1997) suggest that locking needles can help stabilise the prostate to reduce seed misplacement, while Taschereau *et al.* (2000) found no effect of locking needles. Even if locking needles reduce the prostate motion, it is necessary to be able to predict the changes in prostate position and shape to be able to deliver the seeds at the desired position.

In our own study (Lagerburg *et al.*, 2005) we found that only rotation in the coronal plane can be more or less predicted and reduced by the use of locking needles. Rotation in the sagittal plane cannot be predicted or reduced by the use of locking needles.

Alterovitz *et al.* (2003b,a) describe the development of an interactive simulation of needle insertion and radioactive seed implantation in soft tissue to facilitate training and planning for medical procedures. A sensitivity analysis of the simulation parameters was performed. Based on a real medical procedure the default seed placement error was 0.65 cm. The placement error could be reduced to almost zero by inserting the needle 0.65 cm beyond the target depth; this compensates for the tissue deformation. Deviating the insertion height from the target height, to anticipate on tissue deformation, increased the error, while a

sharper needle decreased deformation and hence placement error. Increasing needle insertion velocity decreased the error, due to lower friction forces. The model was relatively insensitive to patient-specific parameters such as global tissue stiffness and compressibility.

In Susil *et al.* (2006) the needles for the insertion of fiducial markers were inserted 5 mm past the target site and then withdrawn back to the intended target depth before depositing the fiducial marker, to reduce the impact of deformation on tissue targeting accuracy.

Adaptation of the needle insertion depth to compensate for tissue motion might help to improve needle and seed placement accuracy, but is a very difficult and inaccurate method, because of the unpredictability of prostate motion (Stone *et al.*, 2002; Lagerburg *et al.*, 2005).

Increase of needle insertion velocity on the other hand, decreases prostate motion, which makes it possible to increase needle and seed placement accuracy. To be able to insert the needle with a high, but controlled, velocity we developed a tapping device (Figure 4.1) (Lagerburg *et al.*, 2006a). With this device the needle is tapped into the prostate, instead of the generally used method of pushing the needle into the prostate. The device will give a certain, well-defined, amount of momentum to the needle. Due to an adjustable needle stop, the needle will be inserted at most a certain, beforehand defined, distance (e.g. 5 mm) into the prostate per tap. This tapping device is the first part of the single needle implant device (SNID), which will be developed at our department and used for MRI-guided brachytherapy (Van Gellekom *et al.*, 2004).

The purpose of this study is to investigate the efficacy of a new needle insertion method in reducing prostate motion. This is done by measuring the prostate movement during needle insertion for two different needle insertion methods, viz. the generally used method of manually pushing the needle and the new method of tapping the needle into the prostate with a prototype robotic system.

(a)   (b)
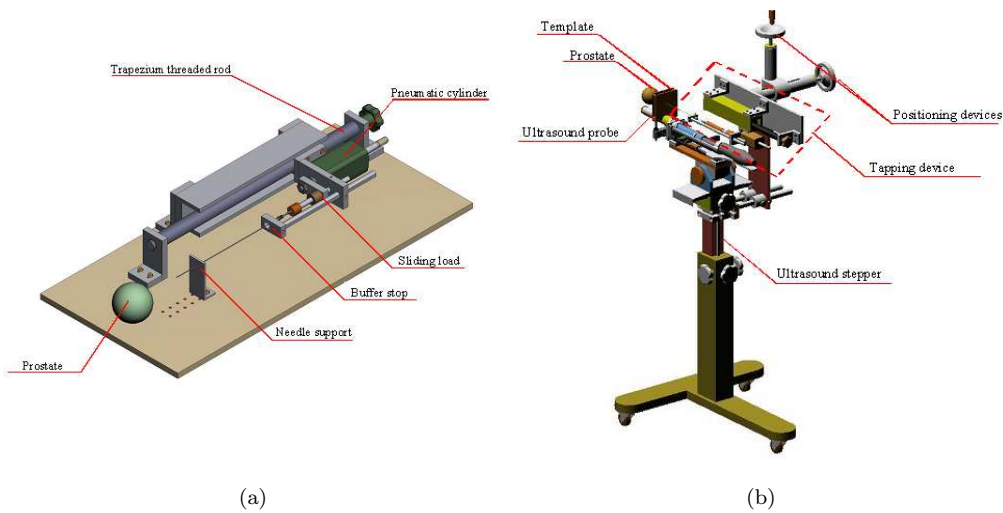
Figure 4.1: Schematic overview of the (a) tapping device and (b) the experimental setup where the tapping device is attached to the ultrasound stepper device.

4.2 Methods and Materials

4.2.1 Implantation procedure

At our institute, patients get gold markers implanted as reliable positioning markers during IMRT (intensity modulated radiation therapy) (Dehnad *et al.*, 2003; Lagendijk *et al.*, 2004). These fiducial gold markers are implanted transperineally about one week prior to CT and MRI acquisition for dose planning. In this study we measured prostate displacement due to needle insertion for transperineal implantation of gold markers in patients receiving prostate IMRT. This group of patients is suitable for this efficacy study for two reasons. Firstly, the exact gold marker position is not critical as long as it is representative for the prostate position and secondly, the insertion of three markers via two needles can be done in an acceptable time even with the experimental tapping device. Since the procedure for the implantation of gold markers is the same as the procedure for prostate brachytherapy we expect similar prostate motion due to needle insertion.

The patient was placed in the lithotomy position and the prostate was visualised using a transrectal ultrasound probe. A rectangular template with 5 mm

spaced holes was positioned against the perineum. The fiducial gold markers were implanted through an iodine-implantation needle. After the desired marker position was determined, the first needle was inserted. The markers were delivered by retracting the needle while maintaining the obturator at its position behind the marker. In total three markers per patient were placed, with two needles. For our study the normal procedure was changed slightly for half of the included patients. Instead of pushing the needle into the prostate, the needle was tapped. The physician pushed the needle through the skin up to just before the prostate. Then the needle was attached to the tapping device (Figure 4.2) and tapped into the prostate until the tip of the needle reached the desired position. With the tapping device it is possible to insert a needle stepwise into the prostate with a certain, well defined, amount of momentum. The momentum is adjustable by changing the air pressure. During this study we started with a pressure of 6 bar, because this was equal to the mean momentum a physician needed to insert a needle into the prostate (Lagerburg *et al.*, 2006a). After the first five patients, we increased the pressure to 8 bar. Pressures of 6 and 8 bar give a momentum of 0.49 ± 0.06 and 0.61 ± 0.08 Ns respectively. The distance that the needle is inserted into the prostate per tap is adjustable by setting the buffer stop (Figure 4.1(a)). We chose a distance of 5 mm for each tap. After the needle reached its desired position, the needle was disconnected of the tapping device and the first gold marker was implanted. Then the needle was manually retracted 1 cm, and the second gold marker was implanted. After this the needle was totally retracted and the next needle was inserted in the same way as the first. The retraction of the needles was always done manually.

During the procedure the ultrasound images in the longitudinal direction were recorded using a video recorder. On these images we are able to see the prostate movement in the cranio-caudal direction during needle insertion and retraction. The ultrasound images contain a virtual template of 5 mm spaced dots, which makes it possible to relate the distances on the video records to the real distances.

4.2.2 Measurement of the prostate motion

Prostate motion and needle insertion depth per tap were measured on the video record of the ultrasound images. Prostate and needle were delineated on the

(a)   (b)
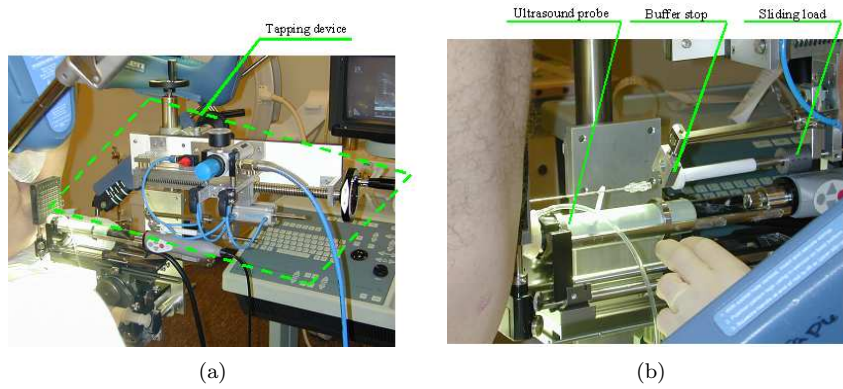
Figure 4.2: Experimental setup of the measurement of prostate motion when the needle is tapped into the prostate with (b) a detailed photo of how the needle is attached to the tapping device

images, just before and after each tap or push. The displacement of the prostate in the cranio-caudal direction is measured at the needle insertion point (Figure 4.3).

(a)   (b)   (c)
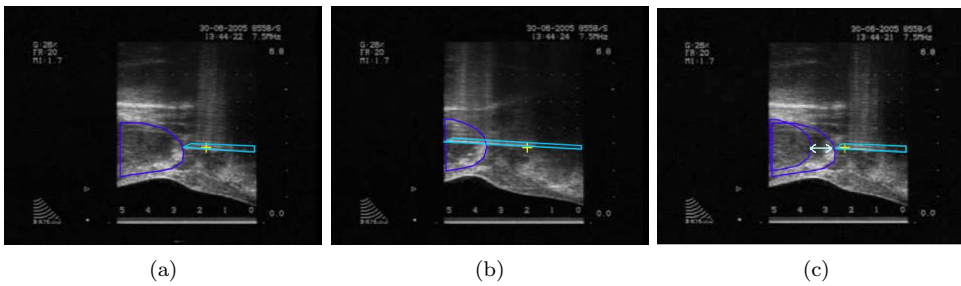
Figure 4.3: Example of how the prostate motion is measured. In (a) the prostate position before pushing is shown, in (b) after pushing and in (c) both prostate contours and the distance between those two is shown

During needle insertion the prostate moves away from its original position. Directly after the needle reaches its pre-planned position and stops moving, the prostate often rebounds, but mostly not to its original position. For this study we measured the prostate displacement both before and after rebound. We decided to only use the prostate displacement after rebound in our analysis,

because this is the distance that the needle tip, and thus the seeds, will be away from its original, pre-planned position due to prostate motion.

The total prostate displacement is the difference between the prostate position before the first tap (or push) and after the last tap (or push) at the needle insertion point. The distance that the needle is inserted into the prostate with every tap (or push) was also measured.

We also measured prostate displacement due to retraction of the needles. In all cases the needles were manually retracted, since the prototype robotic system can only tap forward. Prostate displacement due to retraction is the difference between the prostate position just before and just after retraction of the needle.

The calculated prostate movements were analysed with SPSS using descriptive statistics, the t-test and the Mann-Whitney test.

4.3 Results

The measurements were performed in 30 patients. In total 29 needles were tapped into the prostate and 32 needles were pushed. Due to e.g. air bubbles the quality of some ultrasound images was low and we were not able to use the data of all the patients. In total the insertion of 54 needles was analysed (26 tapped and 28 pushed) for 30 different patients. In Table 4.1 an overview of the results is shown.

The total prostate displacement (from before needle insertion until the needle reached its final destination) when the needle was pushed into the prostate ranged from 0.3 to 21.6 mm with a mean of 5.6 mm. The total prostate displacement when the needle was tapped into the prostate ranged from 0 to 2.0 mm with a mean of 0.9 mm. The mean number of taps used was 8. There was a significant difference found in total prostate displacement between the two needle insertion methods ($p < 0.001$).

The mean needle insertion depth per tap was 4.3 mm for the first five patients. Because we noticed during the experiments that for some patients we were not able to insert the needle the pre-defined distance of 5 mm into the prostate, we increased the air pressure from 6 to 8 bar (0.61 ± 0.08 Ns). After the pressure

was increased to 8 bar the mean needle insertion depth per tap increased to 4.9 mm. The total prostate motion decreased from 1.4 mm to 0.7 mm.

In all cases the needles were manually retracted, which also caused prostate movement. In the group of patients, for which the needles were manually pushed into the prostate, the mean prostate displacement (after rebound) due to needle retraction amounted 1.5 ± 1.5 mm. In the group of patients, for which the needles were robotically tapped into the prostate, the mean prostate displacement due to retraction amounted 0.7 ± 0.6 mm ($p < 0.05$). The increase of the pressure to 8 bar did not significantly influence the prostate displacement during retraction of the needle.

		Mean $\pm$ SD (mm)	Minimum (mm)	Maximum (mm)
Insertion	Pushing	5.6 ± 4.9	0.3	21.6
Insertion	Tapping (6 bar)	1.4 ± 0.6	0.4	2.0
Insertion	Tapping (8 bar)	0.7 ± 0.5	0	1.7
Retraction	Pushing*	1.5 ± 1.5	0	5.5
Retraction	Tapping (6 bar)*	0.8 ± 0.8	0	2.1
Retraction	Tapping (8 bar)*	0.6 ± 0.6	0	2.4

*The needles were always manually retracted, but the group of patients is split according to the way the needles were inserted into the prostate.

Table 4.1: Mean $\pm$ standard deviation, minimum and maximum total prostate movement while pushing or tapping the needle into the prostate and during retracting (always manually) the needle.

4.4   Conclusion and Discussion

Currently the needles for percutaneous needle insertion are pushed into the tissue. Due to the elastic properties of tissue this results in tissue motion. In this study we present a new needle insertion method, viz. tapping the needle into the tissue instead of pushing. This insertion method was tested during the implantation of gold markers for prostate IMRT. With this new needle insertion method, prostate motion is significantly reduced in comparison with the currently used method of pushing the needle into the prostate.

Prostate motion and deformation due to needle insertion were subject of several theoretical and simulation studies (DiMaio and Salcudean, 2002b; Alterovitz *et al.*, 2003b,a; DiMaio and Salcudean, 2002a), but measured data are scarce (Dattoli and Waller, 1997; Stone *et al.*, 2002; Lagerburg *et al.*, 2005).

Dattoli and Waller (1997) found a displacement of the prostate of 1 cm without locking needles and 0.2 mm with the use of locking needles in the lateral direction. Stone *et al.* (2002) found maximum movement of the prostate in the cranial-caudal direction that ranged from 0 to 30 mm (median 15 mm). In the lateral direction a mean displacement of 1.93 and a maximum displacement of 4.61 mm was found. In the anterior-posterior direction a mean displacement of 2.60 mm and a maximum displacement of 5.86 mm was found. Lagerburg *et al.* (2005) measured the prostate rotation during needle insertion. The maximum rotation found was 13.8 degrees. With this rotation and a strand existing of four seeds the maximum displacement of the seeds relative to the planned position that can occur is 8.4 mm.

In this study we found a mean prostate displacement of 5.6 mm when the needle was pushed into the prostate. When the needle was tapped, the mean prostate displacement significantly decreased to 0.9 mm.

From the experiments it became clear that the achieved momentum was not always high enough to insert the needle the pre-defined distance of 5 mm into the prostate. This is caused by the stiffness of the prostate. The counter-pressure was different for every patient and even varied between different insertion points in one prostate. After the first five patients we therefore increased the air pressure from 6 to 8 bar. This resulted in an increase of the distance that the needle was inserted into the prostate per tap from 4.3 to 4.9 mm. A small deviation from the pre-planned distance of 5 mm is possible with this prototype tapping device because the distance is set by hand. Furthermore, we saw a decrease in total prostate displacement from 1.4 to 0.7 mm after the pressure was increased from 6 to 8 bar. This is due to the higher needle insertion velocity and indicates that it is possible to further decrease the prostate displacement when an even higher air-pressure is used. Unfortunately this was not possible with the used prototype.

Since the prototype robotic system can only tap forward, all needles were manually retracted. The prostate displacement due to manual retraction of the needles was less in the group of patients who had the needles tapped into the

prostate compared to prostate displacement in the group of patients who had the needles manually pushed into the prostate. Our hypothesis is, that retraction of the needles makes the prostate more or less return from its changed position due to needle insertion to its original position. This displacement is smaller for the patients who had the needles tapped into the prostate. We expect that prostate displacements will be minimal when the needles are tapped both into and out of the prostate.

In our study we only analysed the prostate movement in one direction. We chose the cranio-caudal direction because we expected the prostate movement to be largest in this direction. In Stone *et al.* (2002) the prostate movement in all three directions was analysed. They were able to do that because they only made ultrasound scans at two distinct time points, before needle insertion and after needle insertion. We wanted to follow prostate motion in time, and therefore only had the availability of two-dimensional scans. The disadvantage of a two-dimensional scan is that it is very difficult to analyse deformations due to needle insertion. The change of prostate shape in the image plane can be seen, but can be caused by deformations as well as movement in the two other directions (in this case the anterior-posterior direction and the left-right direction).

In conclusion, a new needle insertion method to decrease prostate motion during needle insertion is described. Instead of the currently used method of pushing the needle into the prostate, the needle was tapped. This new needle insertion method was tested during the insertion of gold markers into the prostate. A significant decrease in prostate motion was found for this new needle insertion method compared with the old method.

Besides for the insertion of gold markers into the prostate, this new needle insertion method can also be useful in other applications where tissue motion due to needle insertion is problematic such as e.g. breast biopsies (Deurloo *et al.*, 2001).

The next step in this research project will be the development of an automatic MRI compatible tapping device for implantation of gold markers, which is also able to tap the needle out of the prostate, because prostate motion also occurs during retraction of the needle, which might influence seed placement accuracy as well (Krieger *et al.*, 2005).

Chapter 5

Simulation of the artefact of an iodine seed placed at the needle tip in MRI-guided prostate brachytherapy

Abstract The purpose of this research is to study the influence of different needle materials on the artefact of a prostate brachytherapy iodine seed, placed at the needle tip, in MRI(Magnetic Resonance Imaging)-guided prostate brachytherapy. For this research simulations and MRI experiments were performed. Although there were some differences between the simulations and the MR images, the pattern of the MR images was reproduced by the simulations. The simulations showed that with the currently available MRI compatible titanium needles determination of the exact seed position is difficult, because of the large artefact at the needle tip. This hampers accurate MRI-guided seed delivery. When a plastic needle is used, the image disturbance is caused by the artefact of the iodine seed alone. When a GE (Gradient Echo) sequence is used, the middle of the seed artefact corresponds well with the middle of the real seed position. With the scan parameters we used this deviation was less than 0.4 mm compared to 1.5 mm when a titanium needle is used.

5.1   Introduction

Magnetic Resonance Imaging (MRI)-guided interventions offer a great opportunity for different kindof applications, e.g. prostate brachytherapy, prostate biopsies, breast biopsies and vascular interventions (D'Amico *et al.*, 1998; Mahnken *et al.*, 2004; Ménard *et al.*, 2004; Paetzel *et al.*, 2005; Engelhard *et al.*, 2006; Perlet *et al.*, 2006; Susil *et al.*, 2006). Advantages of MRI are the possibility of on-line imaging, the non-attendance of radiation exposure in contrast to CT (Computed Tomography) and the good image quality, especially the soft tissue contrast, compared to ultrasound. This allows tracking of needles or catheters during an intervention and also a better delineation of the prostate and even visualisation of structures inside the prostate in prostate brachytherapy. With new developments in MRI, such as higher field strengths, MR spectroscopy and perfusion, it becomes possible to visualize suspected tumour areas inside the prostate, where an extra dose can be given during treatment. Unfortunately, there are some difficulties in MRI-guided interventions, such as the limited space inside the bore and the forces and torques of the magnetic field on surgical instruments. The attractive forces of the magnetic field make it hazardous to use magnetic materials during the implantation procedure. Non-magnetic materials can be used, but these materials can still give an artefact which degrades the image quality. To overcome these drawbacks we are developing a MRI compatible robotic device for MRI-guided prostate brachytherapy (Van Gellekom *et al.*, 2004; Lagerburg *et al.*, 2006a) and are investigating the use of different needle and stylet materials. The focus of this study is the image artefact of the iodine seed, placed at the needle tip, which is the situation just before seed delivery and the very last moment to adapt its position if necessary. This situation is relevant for techniques using either afterloading or preloaded needles.

Our robotic MRI-guided prostate brachytherapy procedure will be performed as an afterloading technique. This means that the needle with the stylet inside are inserted together to their planned position into the prostate, after which the stylet is retracted and iodine seeds are delivered through the needle. In the first step, needle and stylet artefact influence accuracy of needle placement. This situation was studied by Müller-Bierl *et al.* (2005), who used combinations of titanium and bismuth to make the artefact as small as possible, but especially at the tip, an artefact remained. In the next step, the stylet is retracted and seeds are pushed into the needle up to the tip. The combination of the needle

and seed will alter the artefact. Since this is the moment just before seed delivery, it is important to be able to deduce the exact seed position from the MR image. Constant monitoring of the needle and seed position is mandatory because also in the short time between needle insertion and seed delivery, the needle tip position relative to the prostate anatomy may change due to patient and/or organ motion. Furthermore, needle insertion and needle retraction may lead to prostate deformations that disturb the exact positioning of the iodine seed. Errors in the order of 2 mm in seed delivery may influence the dose distribution in the prostate significantly (Dawson *et al.*, 1994; Moerland *et al.*, 1997). Needle retraction delivers the seeds in the prostate, which are depicted on the MR images as signal voids due to the seed artefacts. Wachowicz *et al.* (2006) performed simulations of the MRI artefact of a brachytherapy seed, which are relevant for intra-operative feedback of seed delivery and MRI-based post-implant dosimetry.

The main objective of this research is to investigate the influence of different needle materials on the artefact of an iodine seed, placed at the needle tip, depending on different orientations to the main magnetic field.

5.2 Methods and Materials

5.2.1 Simulation

Simulations were performed to study the MRI artefact of an iodine seed, placed at the tip of a needle. To simulate an MR image first the B-field distribution must be calculated. There are several methods to calculate this B-field distribution. We used the validated multi-resolution finite difference method that was developed at our own department (Bhagwandien *et al.*, 1994).

In this method the B-field distribution is calculated for an object with known susceptibility distribution. This object is assumed to be placed in a large area such that the field at the boundaries is not influenced by the field distortions induced by the object. First, the magnetic scalar potential (MSP) is calculated at a low resolution. After a stationary solution is achieved, the boundary values are copied from the low-resolution solution and placed closer to the object. Then the calculation is performed again. This multi-resolution method

is performed to reduce computation time (Bhagwandien *et al.*, 1992) and is suited to investigate small details around seeds and needles. With the central difference method the H-field is calculated from the MSP-field, and in the last step the B-field is calculated from the H-field using B $= \mu_0$ (1- (2/3 χ)) H. This method was tested and validated in 2D and 3D using analytically known solutions (Bhagwandien *et al.*, 1994).

From the calculated B-field distribution an MR image can be simulated, which depends on the pulse sequence and scan parameters chosen (Bakker *et al.*, 1994). This method of simulation proved to be a powerful tool for analysing MRI susceptibility artefacts in great detail (Wachowicz *et al.*, 2006).

5.2.2 Methods

The needle that was simulated consists of two parts: an inner solid stylet with a conical tip and an outer hollow needle. The inner stylet has a diameter of 0.95 mm. The outer hollow needle has an inner diameter of 1 mm and an outer diameter of 1.29 mm. These dimensions resemble the dimensions of a commercially available, MRI compatible, 18G titanium needle (Invivo Germany GmbH, Schwerin, Germany), which is suitable for prostate brachytherapy. The simulations were performed with a seed placed at the tip of the needle (see Figure 5.1(a)), the situation just before seed delivery. The radioactive iodine seeds (selectSeed, Isotron, Isotopentechnik GmbH, Berlin Germany) consist of a silver rod with I-125 adsorbed and a titanium encapsulation (Figure 5.1(b)).

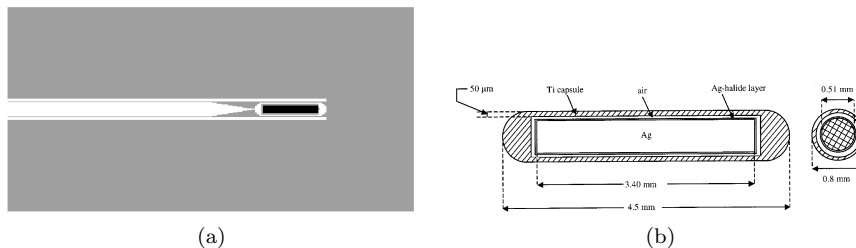(a)   (b)

Figure 5.1: Configuration used for the simulation: (a) needle with a seed placed at the tip, (b) a selectSeed (Karaiskos *et al.*, 2001)

The simulations were performed with the long axis of the needle under different angles with respect to the main magnetic field; 0 (parallel to the B-field), 5, 10

and 15 degrees to the B-field. These angles are within the range of angles that will be used during the brachytherapy procedure (Van Gellekom *et al.*, 2004). The magnetic volume susceptibility of the background was set to -9.0 ppm which is comparable to that of the human tissue.

First, we simulated the seeds alone. The artefact was simulated for two different SE and GE sequences. The first set of parameters was used for comparison with the MRI experiments performed and the second set was used for analysing the artefact. For the first GE sequence, GE(1), the slice selection gradient was operated at 7.553 mT/m, the read out gradient at 11.924 mT/m and the phase encoding gradient was stepped at increments of 0.117 mT/m. For the SE sequence, SE(1), the slice selection gradient was operated at 17.5 mT/m, the read out gradient at 2.566 mT/m and the phase encoding gradient was stepped at increments of 0.117 mT/m. Other relevant parameters are as follows: TR = 500 ms, TE = 30 ms in GE, TE = 40 ms in SE, slice thickness = 10 mm in GE and 1 mm in SE, FOV (Field Of View) = 12.8 x 25.6 x 12.8 mm, number of time samples and phase encoding steps is 256, output matrix (256 x 256). The read-out gradient direction was parallel to the B-field. The used resolution was 0.05 x 0.1 x 0.05 mm.

For the second set of simulations, GE(2) and SE(2), the slice selection gradient was operated at 30 mT/m, the read out gradient at 10.2 mT/m and the phase encoding gradient was stepped at increments of 0.117 mT/m. Other relevant parameters are as follows: TR = 500 ms, TE = 30 ms in GE, TE = 50 ms in SE, slice thickness = 1 mm, FOV (Field Of View) = 12.8 x 25.6 x 12.8 mm, number of time samples and phase encoding steps is 256, output matrix (256 x 256), sampling interval $\Delta t = 90$ μs. The read-out gradient direction was parallel to the B-field. The resolution used was 0.05 x 0.1 x 0.05 mm. These parameters were also used for the simulations of the needle with the seed placed at the tip.

For accurate seed placement, the needle (tip) artefact should be as small as possible. Two different approaches to reduce the needle tip artefact were simulated. The first approach was described in Müller-Bierl *et al.* (2005) and is based on the use of a combination of paramagnetic and diamagnetic materials. In this case, the inner stylet and the outer needle are made of different materials. The level of compensation depends on the amount and volume susceptibility of the materials. The second approach uses just one material, but with a susceptibility closer to tissue than titanium, the material of which the only currently commer-

cially available MRI compatible needles are made. We simulated three different materials for the whole needle: titanium (χ = 182 ppm, as this is the currently used material), aluminium (χ = 20.7 ppm) and plastic (χ = -9.3 ppm). Five different combinations of two materials were used in our simulations: a needle of bismuth (χ = -164 ppm) with a stylet of titanium and vice versa, a needle of plastic and a stylet of tungsten (χ = 77.2 ppm), the same configuration, but with the tip made of plastic, and the same configuration but with the far end of the stylet (tip including an extra centimetre of the stylet) made of plastic.

The influence of the presence of the needle (tip) on the seed artefact was analysed by first investigating the size and position of the seed artefact alone. Subsequently we analysed the influence of the needle (tip) artefact on the seed artefact, by determining the distance between the end of the real seed position and the end of the artefact (see Figure 5.2). The end of the artefact was determined by taking a profile through the middle of the artefact (see arrows in Figure 5.2). For a SE image the artefact includes the pixels with the maximum intensity and ends when the intensity becomes lower than 75 % of this maximum intensity. For the GE image the end of the artefact is at 75 % of the maximum intensity, which is the background intensity. If this distance is changed due to the presence of the needle, it becomes more difficult to determine the exact seed position based on the artefact. To determine the middle of the artefact of a seed alone, the beginning and the end of the artefact are determined in the same way as described above. Based on these values, the middle is determined.
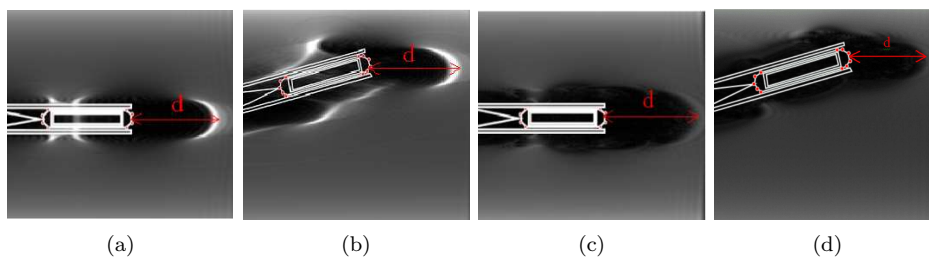

(a)   (b)   (c)   (d)

Figure 5.2: Example of how the distance between the end of the seed and the end of the artefact is measured for (a) a SE scan, (b) a SE scan with the needle and seed under an angle of 15 degrees to the B-field, (c) a GE scan and (d) a GE scan with the needle and seed under an angle of 15 degrees to the B-field

5.2.3 Measurements

To verify the simulations, MR images were made of an iodine seed and of a titanium needle with a seed placed at the tip of the needle. The seed was placed in a phantom with a manganese chloride solution with relaxation times comparable to human tissue values. The needle with the seed at the tip was placed in a rotatable phantom. The phantom was placed on a protractor, allowing positioning of the needle under a well-known angle to the B-field. SE and GE sequences were performed. For the seed experiment relevant scanning parameters for the SE sequence are: read-out gradient = 2.566 mT/m, slice selection gradient = 17.5 mT/m, TE = 40 ms, FOV = 128 x 128 mm, resolution = 0.333 x 0.333 mm, TR = 550 ms. For the GE sequence relevant parameters are: read-out gradient = 11.924 mT/m, slice selection gradient = 7.553 mT/m, TE = 30 ms, FOV = 128 x 128 mm, resolution = 0.25 x 0.25 mm, TR = 38.97 ms and a slice thickness of 10 mm. These parameters correspond to the first set of parameters used for the simulations.

Relevant scanning parameters for the needle with the seed placed at its tip for the SE sequence are: readout bandwidth of 34.5 Hz/pixel, TE = 40 ms, FOV = 128 x 128 mm, resolution = 0.333 x 0.333 mm, TR = 1350 ms. For the GE sequence the relevant parameters are: readout bandwidth of 207.8 Hz/pixel, TE 30 ms, FOV = 128 x 128 mm, resolution = 0.5 x 0.5 mm, TR = 500 ms.

5.3   Results

First we simulated the artefact of an iodine seed for the SE(1) and GE(1) sequences. In Figure 5.3, the results of these simulations and the corresponding MRI scans are shown. The simulations are in good agreement with the one shown in the literature (Wachowicz *et al.*, 2006). Although the actual, non ideal, MRI pulse sequence parameters may differ somewhat from the chosen (ideal) parameters in the simulations, the pattern of the MRI experiments was reproduced by the simulated artefacts. In Figure 5.4 the simulations of the seed for the second set of scan parameters (SE(2) and GE(2)) are shown. These simulations are used for analysing the seed artefact.

From the simulations, it is clear that the seed artefact is larger than the seed itself and the seed is not located in the middle of the artefact. If the seed

position is estimated to be in the middle of the artefact, and the seed is placed parallel to the B-field (read out parallel to the main magnetic field, 10.2 mT/m), the total error (widthwise and in the length direction together; vector sum) is approximately 1.2 ± 0.1 mm for a SE sequence and less than 0.4 ± 0.1 mm for a GE sequence. This error does not seem to vary for the different angles of the seed to the B-field investigated.

(a)   (b)   (c)   (d)

Figure 5.3: Simulation and MRI experiment of an iodine seed for the SE(1) sequence (first row) and the GE(1) sequence (second row) with (a) the B-field distribution, (b) the simulated artefact with the contour of the seed geometry overlaid, (c) the simulated artefact and (d) the MRI scan.

(a)   (b)   (c)   (d)
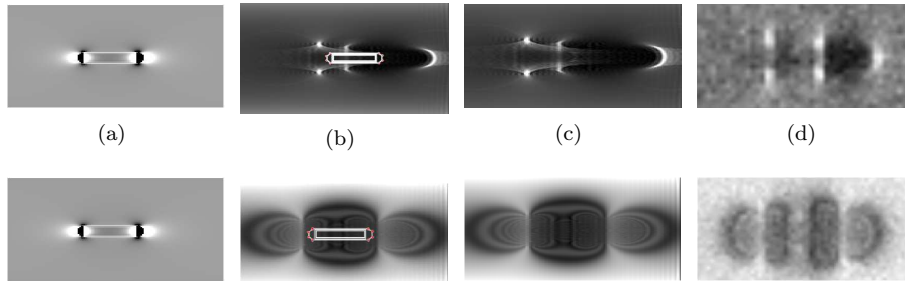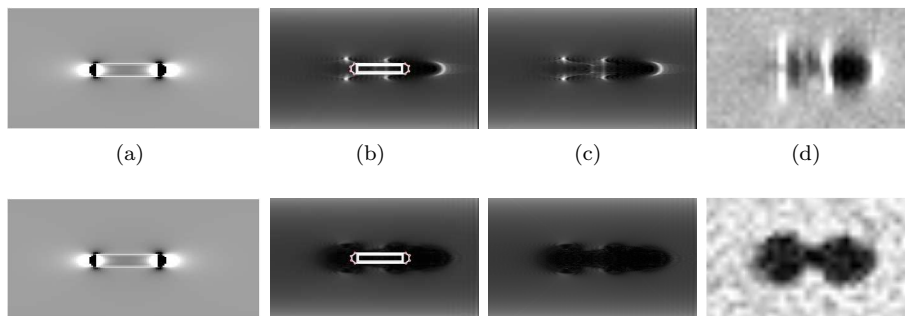
Figure 5.4: Simulation of an iodine seed for the SE(2) sequence (first row) and the GE(2) sequence (second row) with (a) the B-field distribution, (b) the simulated artefact with the contour of the seed geometry overlaid, (c) the simulated artefact and (d) the MRI scan

In Figure 5.5 and 5.6, the results for a titanium needle with a seed placed at its

tip are shown. For the MRI experiments the same scan parameters were used as for the simulations. The figures show that the simulated images and the images from the MRI experiments have some differences, but in general they are comparable. From the simulated images, it becomes clear that the seed artefact is enlarged when it is placed at the tip of the needle. This makes it very difficult to determine the exact seed position from the artefact. The width of the artefact is also enlarged. If the seed position is estimated to be in the middle of the artefact, and the seed is placed parallel to the B-field (read out parallel to main magnetic field, 10.2 mT/m), the total error (widthwise and in the length direction together; vector sum) is approximately 1.1 ± 0.1 mm for a SE sequence and 1.5 ± 0.1 mm for a GE sequence.

(a)   (b)   (c)   (d)

Figure 5.5: Simulation and experiment of the GE(2) scan with a titanium needle and a iodine seed placed parallel to the B-field (first row) and 15 degrees to the B-field (second row) with (a) the B-field distribution, (b) the simulated artefact with the contour of the seed geometry overlaid, (c) the simulated artefact and (d) the MRI scan

In Figures 5.7 and 5.8, the simulation of a GE sequence for different needle materials with the needle parallel and with an angle of 15 degrees to the main magnetic field is shown. Because the seed is placed directly after the stylet tip and inside the hollow needle, the artefact of the needle influences the artefact of the seed. The closer the susceptibility of the material is to the susceptibility of human tissue, the smaller the B-field distortion induced by the needle and the better the artefact of the seed becomes visible. Although aluminium has a susceptibility of only 20.7 ppm (in comparison to titanium with a susceptibility of 182 ppm), the seed artefact is still influenced by the needle artefact and therefore it is still difficult to accurately determine the exact seed position
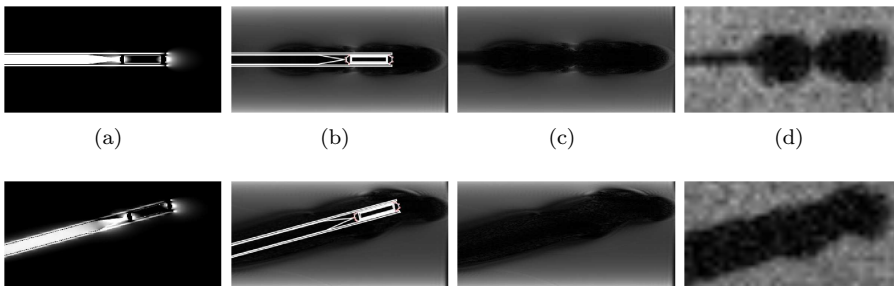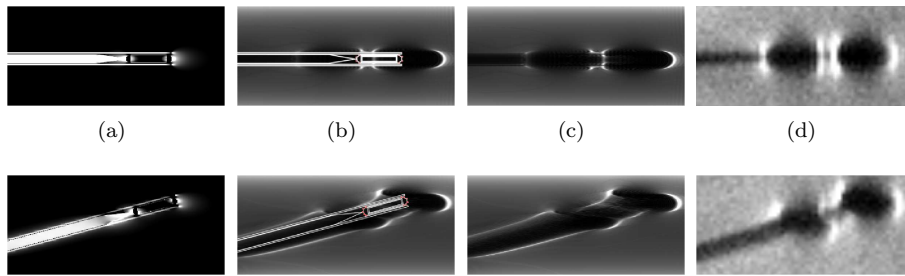
Figure 5.6: Simulation and experiment of the SE(2) scan with a titanium needle and a iodine seed placed parallel to the B-field (first row) and with an angle of 15 degrees to the B-field (second row) with (a) the B-field distribution, (b) the simulated artefact with the contour of the seed geometry overlaid, (c) the simulated artefact and (d) the MRI scan

based on the artefact. With a combination of titanium and bismuth, the artefact becomes smaller in comparison with titanium alone. The best compensation at the end of the needle, where the seed is placed, is achieved when titanium is used for the stylet and bismuth for the needle. The diamagnetic properties of the bismuth needle compensate for the paramagnetic properties of the titanium stylet and the seed which leads to a smaller seed artefact than with a seed alone. The width of the artefact is the same as with a titanium needle. With a bismuth stylet and a titanium needle, the distance between the end of the seed and the end of the artefact is the same as for the titanium needle. The artefact at the beginning of the seed and around the needle itself becomes smaller than for a needle of titanium alone, especially when the needle is placed under an angle to the B-field. When a plastic needle, with a tungsten stylet with a plastic tip is used, the end of the seed artefact is clearly visible. The beginning of the seed artefact remains unclear, because the artefact of the tungsten stylet interferes with it. Only when the needle and stylet (at least the tip and the last part of the stylet) are made of plastic is the seed artefact clearly distinguished.

The artefact becomes larger when the needle is placed under an angle to the magnetic field, which mainly results in broader artefacts. The distance from the end of the seed to the end of the artefact does not seem to vary with the angle to the B-field under which the needle is placed. The distance is dependent on the needle material used and becomes smaller when a material with a susceptibility

close to human tissue is used. With a plastic needle, the distance is equal to the distance without a needle around the seed.
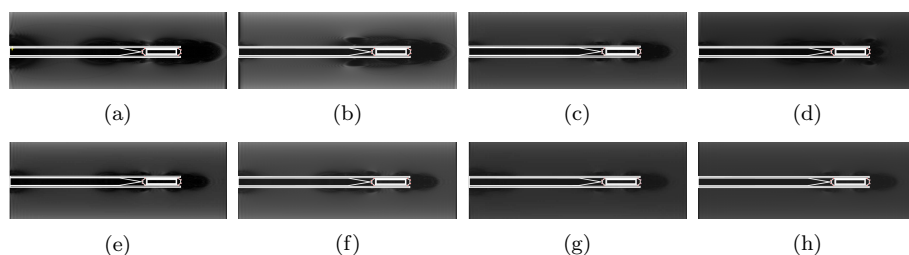
Figure 5.7: Simulation of the artefact for the GE(2) scan of a needle with an iodine seed placed parallel to the B-field for different needle materials (a) titanium, (b) bismuth stylet with titanium needle, (c) aluminium, (d) titanium stylet with bismuth needle, (e) tungsten stylet with plastic needle, (f) tungsten stylet with plastic tip and with plastic needle, (g) tungsten stylet with the far end of the stylet (tip including an extra centimetre of the stylet) of plastic and with a plastic needle, (h) plastic.

5.4 Conclusion and Discussion

In this simulation study we investigated the influence of different needle materials on the MR image artefact of an iodine seed, placed at the needle tip. This reflects the situation in a brachytherapy procedure just before seed delivery, and therefore the very last moment to adapt its position if necessary. The simulations showed that with the currently available MRI compatible titanium needles determination of the exact seed position is difficult, because of the large artefact at the needle tip. This hampers accurate MRI-guided seed delivery. The use of a plastic needle reduces image disturbance to the artefact of the iodine seed alone. When a GE sequence is used, the middle of the seed artefact corresponds well with the middle of the real seed position. With the scan parameters we used, and with a plastic needle, this deviation was less than 0.4 mm.

Our MRI scans show some differences with our simulations. There are several possible explanations for these differences, such as digitisation of the geometry, which has especially its influence at the end of the seed where the titanium
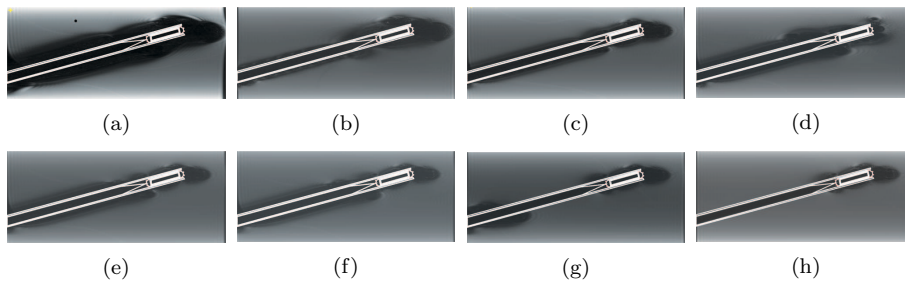
Figure 5.8: Simulation of the artefact for the GE scan of a needle with an iodine seed placed with an angle of 15 degrees to the B-field for different needle materials (a) titanium, (b) bismuth stylet with titanium needle, (c) aluminium, (d) titanium stylet with bismuth needle, (e) tungsten stylet with plastic needle, (f) tungsten stylet with plastic tip and with plastic needle, (g) tungsten stylet with the far end of the stylet (tip including an extra centimetre of the stylet) of plastic and with a plastic needle, (h) plastic.

welds are located and at the needle tip, differences in resolution between the simulations and experiments, slice selections effects and excitation effects.

In general it is very difficult to define a good measure to describe artefacts, because the artefact is dependent on the scan parameters chosen and the window/level adjustments. In our study, we used the distance between the end of the real seed and the end of the artefact as measure. Although the absolute values of this measure are dependent on the scan parameters chosen, the patterns show that the artefact is largest when a titanium needle is used, becomes smaller with an aluminium needle, and with a plastic needle the seed artefact is not enlarged at all.

The artefact of a titanium needle can be reduced by compensating the paramagnetic properties of the titanium seed encapsulation and the stylet by the diamagnetic properties of a bismuth needle. In this case, the artefact is reduced. The disadvantage of this compensation approach is that there are only a few materials that are diamagnetic. Bismuth, the material suggested by Müller-Bierl *et al.* (2005), is a very weak material which makes it difficult to manufacture a needle from it. Furthermore, compensation at the tip is very difficult, because the amount of compensating material has to be adapted to the decrease in material at the tip. Another approach is to use a needle material

with a susceptibility close to that of human tissue, e.g. plastic. The resulting artefact at the needle tip then comes from the seed only. This makes it possible to see the artefact of the seed without interference of the artefact of the needle. An additional advantage of a plastic needle and stylet is that plastic is a non-conductive material; therefore no heating due to RF waves can occur (Konings *et al.*, 2000). A disadvantage of using plastic needles is the lack of hardness compared to the commonly used stainless steel needles.

Artefacts are smaller in SE imaging, but this situation is less relevant since we intend to use fast GE sequences for real time needle tracking during the brachytherapy procedure. Despite the larger artefact, exact seed positioning can be performed more accurately for GE imaging than for SE imaging, since the deviation between the middle of the real seed position and the middle of the artefact is very small. This is only valid when the seed artefact is not disturbed by the needle artefact, and will therefore not work when a titanium needle is used. The ideal would be a seed which gives no artefact, but just a signal void as large as the seed itself. In this way it would be possible to determine the exact position of the seed, without the need of using an indirect method. In this respect, the development of seeds with polymer encapsulation is interesting and might reduce the artefact to a signal void with the exact size of the seed (Bernard and Vynckier, 2005).

To overcome the lack of hardness of a plastic needle and stylet, we are currently working on the development of an MRI compatible needle with a plastic outer hollow and a tungsten stylet of which the far end (tip and last few centimetres) is made of plastic. Tungsten also gives artefacts, but not in the region of interest since the far plastic end does not disturb the image. At the moment of seed delivery, the artefact is only caused by the seed and easily recognized.

In conclusion, with the currently available MRI compatible titanium needles determination of the exact seed position is difficult because the MRI artefacts at the needle tip are large. This artefact hampers accurate seed placement. The use of a plastic needle reduces the artefact to the artefact of the iodine seed alone. When a GE sequence is used, the middle of the seed artefact corresponds well with the middle of the real seed position. For the scan parameters we used, this gives a deviation of less than 0.4 mm compared to 1.5 mm when a titanium needle is used.

Chapter 6

The development of a robotic device for MRI-guided prostate brachytherapy inside a closed bore scanner

Abstract In this study the development and the first MRI compatibility tests of a prototype robotic device are described. This device is developed for Magnetic Resonance Imaging (MRI)-guided prostate brachytherapy inside a closed bore scanner. The robotic device consists of two main parts; one part for the positioning of the device and the needle, and one part to insert the needle into the prostate. To diminish prostate motion during needle insertion, the robotic device makes use of a new needle insertion method. Instead of the currently used method of pushing, the needle is tapped into the prostate. To ensure MRI compatibility the device is pneumatically and hydraulically driven and made of non-magnetic materials. The MRI compatibility tests showed that the magnetic field did not have any influence on the functionality of the robotic device and that the device itself did not cause any artefacts.

6.1   Introduction

Permanent prostate brachytherapy is one of the treatment options for prostate cancer. With brachytherapy it is possible to deliver an adequate radiation dose to the prostate while sparing critical surrounding organs like e.g. the rectum and the neurovascular bundles, due to the sharp dose gradient (Merrick *et al.*, 2001; Stone and Stock, 2002; Merrick *et al.*, 2003b). Source placement precision is of importance, because deviations from the pre-planned position can effect the dose distribution significantly (Dawson *et al.*, 1994; Moerland *et al.*, 1997). To accurately place the seeds, imaging of the prostate, the needle and the seeds during the implantation procedure is necessary. Currently the brachytherapy procedure is performed under ultrasound guidance.

Compared to ultrasound Magnetic Resonance Imaging (MRI) offers a better image quality, especially for soft tissues, which makes a better visualisation of the prostate, and even of structures inside the prostate, possible (Cheng and Tempany, 1998; Husband *et al.*, 1998; Rasch *et al.*, 1999; McLaughlin *et al.*, 2005; Villeirs *et al.*, 2005a). New imaging techniques, such as MR spectroscopy, diffusion-weighted imaging and perfusion, make it possible that in the future suspected tumour areas can be visualised (Scheidler *et al.*, 1999; Buckley *et al.*, 2004; Haider *et al.*, 2007; Reinsberg *et al.*, 2007). These areas can be given a higher dose to increase tumour control probability.

Disadvantages of MRI are the limited amount of space inside a closed bore scanner and the magnetic forces and torques on surgical instrumentation caused by the magnetic field. This makes it necessary to adapt the currently used methods and materials. A robotic device would be a solution for the limited amount of space, but, because of the magnetic field, special care has to be taken which materials are used. Advantages of the use of robotic devices are high accuracy and reproducibility and in the case of brachytherapy also less radiation for the staff.

Some research groups are already working on the development of systems for MRI-guided prostate interventions inside a closed bore scanner. Beyersdorff *et al.* (2005) and Engelhard *et al.* (2006) developed a device for MRI-guided transrectal prostate biopsy. Both showed the feasibility of the device in clinical practice. Susil *et al.* (2003, 2004, 2006) developed a robotic device that is suitable for several prostate interventions among which prostate brachytherapy. The device is suitable for transrectal and transperineal access to the prostate.

The transrectal device was tested on four canines. Three different procedures were accomplished, i.e. needle placement, intraprostatic injection (simular to targets in the needle placement study, targets for an injection in the prostate were selected), and brachytherapy seed placement. In all cases the needles could be accurately placed in the prostate. For the transperineal access the patient was placed in the left lateral decubitus position, to maximise perineal exposure. After imaging and planning of the targets, the patient table is withdrawn from the scanner to insert the needles or catheters. Then the patient is advanced back into the scanner to confirm the placement of the needles. The device has been succesfully tested for biopsies and HDR catheter placement. Muntener *et al.* (2006) and Patriciu *et al.* (2007) developed a fully automated robotic system for brachytherapy seed placement. Some pre-clinical tests were performed to test the feasibility of the system. Although more extensive testing is necessary, the system seems to be promising with a seed placement accuracy of 0.72 ± 0.35 mm in a phantom.

At our own department we are currently working on the development of a robotic device for MRI-guided transperineal prostate brachytherapy. Because of the limited space inside a closed bore MRI scanner, which makes the lithotomy position impossible, and placing of the perineal template difficult, the robotic device makes use of a new implantation procedure, the single needle implant method (Van Gellekom *et al.*, 2004). This single needle is inserted through a rotation point, close behind the skin, and then inserted into the prostate. After delivery of the planned amount of seeds per needle trajectory, the needle is retracted to the rotation point and re-inserted into the prostate, with a different insertion angle. The treatment plans made with the single needle method showed the possibility to cover the prostate with the prescribed dose without piercing the urethra or rectum and without pubic bone interference. This new needle insertion method makes it possible that the patient stays in the scanner during the whole procedure. The influence of prostate motion during needle insertion on the seed placement accuracy becomes even more important with this new implantation method than with the currently used implantation method. With the currently used method first all needles are inserted before seed delivery, so prostate motion between delivery of the seeds is limited. With the new method prostate motion is possible during the insertion of every needle. Since prostate movement is one of the causes of seed displacement during the implantation procedure (Roberson *et al.*, 1997), this

has to be taken into account when performing a brachytherapy procedure. Unfortunately this motion is more or less random (Lagerburg *et al.*, 2005) and therefore difficult to predict. For that reason it is more useful to diminish the prostate motion than try to take the motion into account during the planning procedure.

The robotic device we developed, makes use of a new needle insertion method (Lagerburg *et al.*, 2006a). With this new needle insertion method the needle is tapped into the prostate with a known, well-defined, amount of momentum, instead of the currently used method of pushing. The needle insertion velocity is dependent on the momentum, which can be adjusted by changing the air pressure. Prostate motion during needle insertion is significantly reduced (Lagerburg *et al.*, 2006b) with this tapping device from 5.6 mm when the needle is pushed into the prostate to 0.9 mm when the needle is tapped. With higher momentums we expect prostate motion to decrease even more.

In this study the development, the first MRI compatibility tests and some future plans for the pre-clinical experiments of the robotic device are described.

6.2   Methods and Materials

6.2.1 The robotic device

The robotic device we developed consists of two main parts: one part for positioning of the insertion device and the needle, and one part for insertion of the needle into the prostate (see Figure 6.1). The positioning part consists also of two main parts: a construction for the placement of the whole robotic device relative to the prostate, and an arch on which the insertion part is mounted. At the start of a procedure the robotic device is placed in the right position. During the continuation of the procedure, this part is not moved anymore. The arch is used to adjust the angle of the insertion part, and thereby the needle insertion angle. The movements of the arch are all centric around the needle insertion point. In Figure 6.2 the degrees of freedom of the positioning part are shown. The whole robotic device can be translated in the x, y, and z-direction. The arch can be rotated 360 degrees around its fixing point and it can be moved up and down (20 degrees in both directions, in total an angle of 40 degrees can

be covered). With these two arch movements it is possible to cover the whole prostate.

(a)   (b)
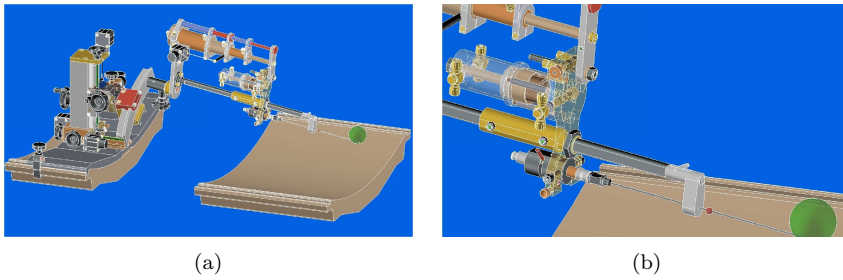
Figure 6.1: Schematic overview of (a) the robotic device with (b) a detailed picture of the tapping device
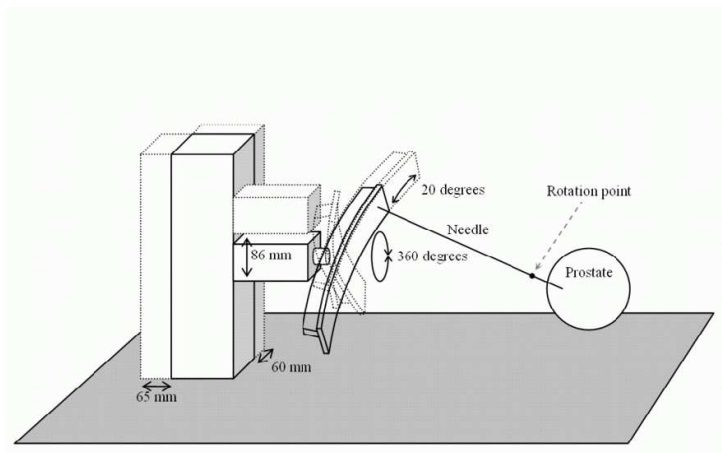
Figure 6.2: Schematic overview of the degrees of freedom of the positioning part of the robotic device

The main elements of the insertion part are a telescopic cylinder, a buffer stop and a tapping device. The tapping device is based on the principle described in Lagerburg *et al.* (2006a) and is able to tap the needle in and out of the prostate. A sliding load is moved forward by a pneumatic cylinder. After the pneumatic cylinder reaches its maximum stroke the sliding load moves further with a constant velocity and hits the needle at which the momentum of the sliding load is transferred to the needle. Driving forces are air pressure for tapping the needle into the prostate and vacuum for tapping the needle out of

the prostate. The maximum insertion depth is 20 cm, which equals the length of the used needles. The telescopic cylinder is used to move the tapping device forward after each tap and to set the distance that the needle can be inserted into the prostate with every tap. The telescopic cylinder is moved with the help of a hydraulic system. The buffer stop is built in to prevent the insertion depth to exceed the previously defined distance. The main materials used for this robotic device are aluminium, brass, and plastic. An 18G MRI compatible titanium needle (Invivo Germany GmbH) was used in our experiments.

6.2.2 The implantation procedure

To perform an implantation procedure with the robotic device several changes are necessary compared to the currently used procedure. The patient lies in the MRI scanner in the supine position with his knees slightly bent, to have maximal access to the prostate. First an MRI scan will be performed to determine the optimal rotation point for the needle. This point is chosen such that access to the prostate is maximal without perforating the urethra, the rectum or the pubic arch. Then the MR images are used to calculate needle angles and seed positions for an optimal dose distribution. The robotic device is placed between the patients legs, such that a needle would pass in a horizontal line through the rotation point (to secure maximum insertion angles in all directions). The arch positions the needle at one of the pre-planned angles and the needle will be tapped a pre-defined distance into the prostate. During the insertion MRI scans will be made to track the needle. If necessary, small corrections can be made to the insertion trajectory. When the needle reaches its desired position, the seeds will be delivered and the needle will be retracted stepwise to the rotation point. Then the insertion angle can be adapted to perform the next needle insertion.

6.2.3 MRI compatibility tests

The MRI compatibility tests of the robotic device exist of two parts. The working of the device in a magnetic field was tested and then MR images were made to investigate whether the device causes image artefacts. To test the working of the device a needle was tapped a pre-defined distance into a piece of cheese. This was done outside and inside the MRI scanner to study the influence of

the magnetic field on the insertion distance. In Figure 6.3 the experimental setup is shown. Hereafter MRI scans were made, both SE (Spin Echo) and GE (Gradient Echo), because both will be used during the brachytherapy procedure. Scans of a piece of cheese were made without the device in the scanner and with the device in the scanner. Influences on the MR images were analysed visually.

(a)

(b)
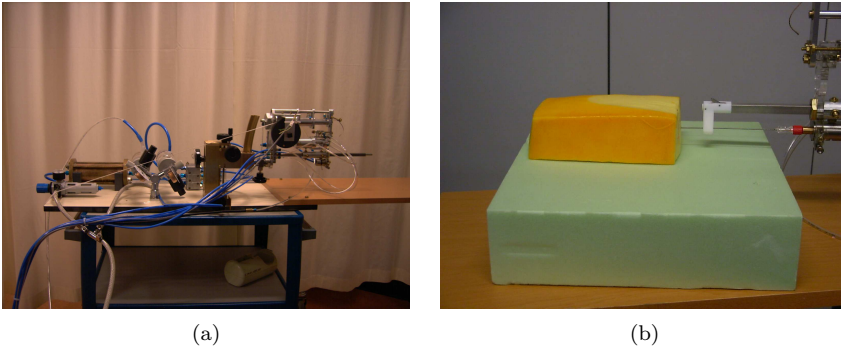
Figure 6.3: Pictures of (a) the robotic device used during the MRI compatibility tests and (b) the experimental setup with the piece of cheese

6.3 Results

To test the working of the robotic device in a magnetic field, a needle was inserted into a piece of cheese. Ten taps were given to the needle which should result in a maximum needle insertion depth of 5 cm (0.5 cm per tap). Both outside and inside the scanner the robotic device was able to insert the needle the maximum distance of 5 cm.

In Figure 6.4 the results of the MRI experiments are shown. Gradient echo images of a piece of cheese were acquired once while the robotic device was outside the scanner room (Figure 6.4(a)) and once with the robotic device inside the MRI scanner (Figure 6.4(b)). The image artefacts in these pictures stem from the cavities in the cheese (solid arrows) and the titanium needle (striped arrow). Apart from these artefacts, comparison of Figures 6.4(a) and 6.4(b) did not show signal loss or shape deformations induces by the robotic

device, from which we conclude that the device did not detoriate the image quality.

(a) (b)
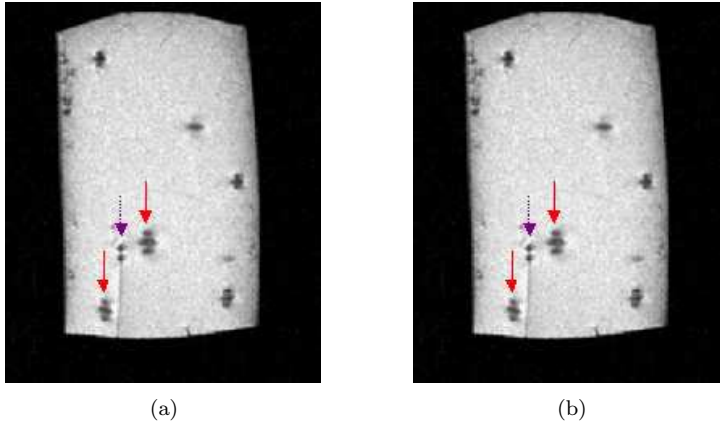
Figure 6.4: MR images of a piece of cheese (a) with the robotic device outside the MRI scanner room and (b) with the robotic device inside the MRI scanner

6.4 Conclusion and Discussion

A robotic device for MRI-guided prostate brachytherapy was developed. MRI compatibility tests showed that the working of the robotic device was not influenced by the magnetic field of the MRI scanner, and that it did not have any influence on the image quality. In upcoming pre-clinical tests we will test the functionality of the device.

Various research groups are working on the development of robotic devices for MRI-guided interventions. As far as the authors know, only two groups are especially working on the development of a device for MRI-guided prostate brachytherapy (Susil *et al.*, 2004; Muntener *et al.*, 2006; Patriciu *et al.*, 2007). Both groups place the patient in the left lateral decubitus position to maximise perineal exposure. A major concern with this position for a longer period is the stability of the patient and the potential for brachial plexopathy and injuries to cutaneous pressure points. In a feasibility study (Van Gellekom *et al.*, 2004) we showed that it is possible to cover the whole prostate with the patient in

the supine position with the legs bent, when the new diverging single needle insertion method is used.

In Susil *et al.* (2004) the patient is moved in and out the scanner to position the needles. With this method no real-time control of the needle position is possible. When the needle is not positioned correctly it has to be re-positioned and checked again, which is a time-consuming procedure. With both our robotic device and the one from Muntener *et al.* (2006) the patient stays in the scanner during the whole procedure. A major difference between the last mentioned device and the one we developed is the needle insertion method. In a previous study we saw that prostate motion is large during needle insertion, which can influence the dose distribution significantly. To solve this problem we tap the needle into the prostate. While tapping the needle into the prostate constant monitoring of the needle position is allowed. Muntener *et al* push the needle with a constant velocity into the prostate, which resembles the currently used method, which is sensitive to prostate motion.

Thanks to the new needle insertion method and the MRI-guidance we think that more accurate seed placement, boosting of tumour volume, and sparing of critical structure is possible, which makes a better dose distribution possible than currently achieved. In the near future we will perform some pre-clinical experiments to test the functionality, and the needle and seed placement accuracy of the prototype robotic device.

Future developments include the automatic supply of the iodine seeds and the adaptation of the device for prostate and breast biopsies.

Chapter 7

Summary and General Discussion

This thesis describes the first steps in the development of a single needle implant device (SNID) for Magnetic Resonance Imaging (MRI)-guided prostate brachytherapy. Its unique design originates from the wish to make use of the excellent image quality of MRI and achieve accurate seed placement. Because of the superior soft tissue contrast of MRI compared to ultrasound, and new developments in MRI such as higher field strengths, dynamic and spectroscopic imaging, it becomes possible to visualise tumour inside the prostate, which can then be given a higher dose. In combination with the accurate seed placement of the SNID, the dose distribution in the prostate can be optimised.

The limited space inside the closed bore MRI scanner makes it impossible to place the patient in the lithotomy position and placement of the perineal template is very difficult. Therefore it is necessary to adapt the currently used implantation technique. Manual needle insertion is possible but the patient has to be moved in and out the scanner repeatedly. This problem is avoided with the use of a robotic implant device that fits in the MRI scanner between the legs of the patient. The SNID makes use of the single needle implant method to perform the implantation procedure (Van Gellekom *et al.*, 2004). With this method one needle is used during the whole procedure. This needle is inserted into the prostate through a rotation point, close behind the skin. After the seeds are delivered, the needle is retracted to the rotation point and re-inserted with a different insertion angle. This in contradiction to the currently used method where first all needles are inserted into the prostate, parallel to each other, after which the seeds are delivered. With the single needle implant method no use

is made of a template or locking needles. An additional advantage of this new implantation technique might be less trauma of the perineum, because there is only one skin entry point.

Prostate motion due to needle insertion is one of the causes of seed displacement. Because a deviation of the seed position with respect to the pre-planned position can influence the dose distribution significantly (Dawson *et al.*, 1994; Moerland *et al.*, 1997) it is of importance to know how (much) the prostate moves during needle insertion. For the development of the SNID this is even of more importance because the single needle implant method is more sensitive to prostate motion than the currently used method where all needles are inserted before seed delivery. This is due to the fact that only one needle is used to deliver the seeds, which is retracted and re-inserted after each seed delivery. This makes prostate motion between every new needle insertion possible, which might influence the seed positions.

In chapter 2 the rotation of the prostate due to needle insertion is investigated. The rotation was measured in two planes, the coronal and sagittal, with and without the use of locking needles. Locking needles are currently used in a lot of hospitals to diminish prostate motion during needle insertion, although in literature no agreement exists on the efficacy of these needles (Dattoli and Waller, 1997; Taschereau *et al.*, 2000; Stone *et al.*, 2002). In our study we found an influence of the locking needles in the coronal plane. With locking needles, the maximum rotation was significantly reduced from 13.8 to 7.8 degrees. In the sagittal plane no influence of the locking needles was found. A prostate rotation of 13.8 degrees results in a seed deviation of 8.4 mm from the pre-planned position when a strand of four seeds is used. In literature some research of seed deviation is described. Kaplan *et al.* (2004) describe in their study the precision of seeds deposited as loose seeds versus suture embedded seeds. They found a mean radial deviation of 3.1 mm with loose seeds and 3.7 mm with suture embedded seeds. Roberson *et al.* (1997) found a source placement error relative to the pre-planned position of 4.6 ± 1.8 mm and Taschereau *et al.* (2000) found a seed displacement of 6.1 mm with locking needles and 6.3 mm without locking needles.

Even with locking needles we found a maximum rotation of 7.8 degrees in the coronal plane. This rotation causes a seed displacement which can influence the dose distribution in the prostate significantly. Because the rotation is more

or less random, especially in the sagittal plane, there is no practical solution to take the rotation into account during planning of the treatment. Therefore other solutions are necessary to accurately place the seeds and optimise dose distribution. A possible solution to decrease seed placement errors might be the diminishing of prostate motion.

To decrease prostate motion during needle insertion a new needle insertion method was developed, namely tapping the needle into the prostate instead of pushing. When the needle is tapped into the prostate, with a high velocity, we expect the prostate motion to diminish. Another solution to decrease prostate motion during needle insertion is drilling the needle into the prostate using vibratory actuation (Yang and Zahn, 2004). A disadvantage of this method might be possible tissue damage due to frictional interactions between the needle and skin.

In chapter 3 the development of a tapping device is described. This device is able to insert a needle into the prostate with a certain, well-defined, amount of momentum. In a dimensioning study, we measured the momentum needed to insert a needle into the prostate. A physician tapped a needle into the prostate while a pressure sensitive membrane (Flexiforce A201 sensor, Tekscan) was attached to the end of the needle. The momentum used to tap the needle into the prostate varied from 0.13 ± 0.02 Ns to 1.16 ± 0.15 Ns with a mean momentum of 0.50 ± 0.07 Ns. The large spread in used momentum corresponds with a large spread in distance that the needle was inserted into the prostate per tap (4.25 mm to 17.5 mm with a mean of 7.9 mm). For the first tap there was a significant correlation between the momentum used and the distance that the needle was inserted into the prostate. After the first tap the distance that the needle was already inserted into the prostate affected the needed momentum, due to friction between the needle and the prostate tissue.

As far as we know there is no literature regarding the momentum necessary to insert a needle in tissue. There is, however, literature regarding the force that is required. Podder *et al.* (2006) e.g. found a maximum needle insertion force of 8.9 N. From the figures in this article, it is possible to calculate a mean momentum. The mean force for the first 4 cm is about 5 N and the mean velocity is 0.3 m/s. With these numbers a mean momentum of 0.67 Ns is found, which is in the same range as the mean momentum we found in our study.

We chose for a momentum-driven system because it is inherently safer than

a force-driven system. If the needle e.g. hits a bony structure the needle will transfer its momentum and stop moving, whereas in a force-driven system the needle will penetrate the bony structure.

The tapping device exists of a pneumatic cylinder (Festo ADVULQ-25-40-A-P-A-S20, Delft, The Netherlands) with a maximum stroke of 40 mm. The pneumatic cylinder moves forward while pushing a sliding load. After the pneumatic cylinder reaches its maximum stroke the sliding load moves further with a constant velocity and hits the needle. The maximum insertion depth of the needle per tap is adjustable and a buffer stop is built in to prevent the insertion depth to exceed the previously defined distance. The maximum velocity of the pneumatic cylinder and thus the needle insertion velocity are adjustable by changing the air pressure and the weight of the sliding load. The tapping device was tested on a piece of beef. During the tests we noticed that the higher the pressure of the pneumatic cylinder, and thus the needle insertion velocity, the less beef motion. Unfortunately we were not able to increase the pressure above 4 bar (corresponds with a momentum of 0.37 Ns) which was still less than the mean momentum used by the physician. With this pressure, and a sliding load of 121.6 gram, a mean movement of 1 mm (range 0 to 2 mm) and a mean rotation of 1.3 degrees (range 0 to 6 degrees) was found. All needles were at least 4 cm inserted into the beef. With a higher pressure we expect even smaller beef movements.

After the phantom experiments a clinical study was performed to compare prostate motion during needle insertion for pushing and tapping the needle into the prostate. In chapter 4 this study is described. The tapping device was adjusted so that it could be attached to the ultrasound stepper that is used in clinical practice. Prostate motion in the cranio-caudal direction was measured on video records of the ultrasound-guided needle insertion procedure. Prostate motion was defined as the distance between the position of the prostate before needle insertion and the position of the prostate after the needle reached its desired position. The mean prostate motion was 5.6 mm (range 0.3 to 21.6 mm) when the needle was pushed into the prostate and 0.9 mm (range 0 to 2.0 mm) when the needle was tapped ($p < 0.001$). For the first patients we used an air pressure of 6 bar. This pressure gives a momentum of 0.49 ± 0.06 Ns which corresponds with the mean impulse a physician needed to insert a needle into the prostate. After noticing that in some cases we were unable to insert the

needle the pre-defined distance of 5 mm per tap into the prostate, we increased the pressure to the maximum value for this prototype, i.e. 8 bar, corresponding with a momentum of 0.61 ± 0.08 Ns. With increasing the pressure from 6 to 8 bar the mean prostate movement decreased from 1.4 mm to 0.7 mm. We expect that prostate movement will be further reduced when the tapping device is operated at higher momentums.

Because we wanted to follow prostate motion in time, we were only able to visualise prostate movement in one direction. Therefore it was not possible to draw any conclusions regarding prostate deformations or rotations during needle insertion. Stone *et al.* (2002) analysed prostate movement in all three directions, but used static scans made at two distinct time points. They found maximum movement of the prostate in the cranial-caudal direction that ranged from 0 to 30 mm (median 15 mm). In the lateral direction a mean displacement of 1.93 and a maximum displacement of 4.61 mm was found. In the anterior-posterior direction a mean displacement of 2.60 mm and a maximum displacement of 5.86 mm was found. Dattoli and Waller (1997) found a displacement of the prostate of 1 cm without locking needles and 0.2 mm with the use of locking needles in the lateral direction.

To be able to deliver the iodine seeds at the pre-planned position a good image of the prostate, the needle and the seeds is necessary. MRI offers a good soft tissue contrast which makes it possible to define structures inside the prostate. The disadvantage of MRI is the necessity to adapt the normally used methods and materials because of the limited space inside the closed bore and the forces and torques of the magnetic field on surgical instruments. The only currently available commercial MRI compatible needles are made of titanium, which still gives a rather large artefact at the tip. A titanium needle with an outer diameter of 1.3 mm (the size of a normally used brachytherapy needle) e.g. gives an artifact at its tip of about 4 mm when the needle is placed parallel to the B-field (1.5 T, GE (Gradient Echo)). This makes it difficult to determine the exact position of the delivered seeds (dimensions 4.5 x 0.8 mm), which is of importance for accurate dose delivery in the prostate. In chapter 5 a simulation study was performed to investigate the artefact of an iodine seed placed at the needle tip. The influence of different needle materials on the seed artefact was also studied. The needles were placed under different angles to the main magnetic field as will be the case during the implantation procedure

when the new single needle implant method is used. For this research first the B-field distribution was calculated making use of the finite difference method. Subsequently this B-field distribution was used to calculate the artefact. For this purpose a precise definition of the scan parameters is required. Simulations were compared with MR images for the iodine seed itself and for a titanium needle with a seed placed at its tip. We first examined the size and position of the seed artefact. Subsequently the influence of the presence of the needle (tip) on the seed artefact was analysed by determining the distance between the end of the real seed position and the end of the artefact. If this distance is changed due to the presence of the needle, it becomes more difficult to determine the exact seed position based on the artefact.

The simulations were in good agreement with the one shown in literature (Wachowicz *et al.*, 2006). The MRI experiments showed some differences with the simulations, but the main pattern was the same. The distance from the end of the artefact to the end of the seed did not vary for the ranges of angles investigated. The distance depends on the needle material used and becomes smaller when a material with a susceptibility more close to human tissue is used. Although aluminium has a susceptibility of only 20.7 (in comparison to titanium with a susceptibility of 182) the seed artefact is still influenced by the needle tip artefact and therefore it is still difficult to accurately determine the exact seed position based on the artefact. With a titanium needle the seed artefact is overwhelmed by the needle artefact, which makes it very difficult to determine the exact seed position. Only with a plastic needle and a stylet with at least the far end and the tip made of plastic, it is possible to distinguish the seed artefact. Although a GE sequence gives a larger artefact than a SE sequence, exact seed positioning can be performed more accurately for GE imaging, since the middle of the seed artefact and the middle of the real seed position correspond well. This gives a deviation in the seed position of less than 0.4 mm for the scan parameters we used.

Müller-Bierl *et al.* (2005) describe a method to compensate for paramagnetic properties by adding diamagnetic material. They simulated a paramagnetic cylinder (out of titanium, $\chi = 181.1$) coated with a diamagnetic layer (out of bismuth, $\chi = -165.0$). The field outside the needlelike instrument was best compensated when the cross-sectional area of the cylinder, multiplied by the absolute susceptibility value of the cylinder material, is equal to the cross-

sectional area of the coating, multiplied by the absolute susceptibility value of the coating material. A disadvantage of this method is that there are only a few materials that are diamagnetic. Bismuth, the material used by Müller-Bierl *et al.* is a very weak material which makes it difficult to manufacture a needle from it. Furthermore, compensation at the tip is very difficult.

In chapter 6 the development of the first prototype of the MRI compatible robotic device is described. The robotic device consists of two main parts: a positioning part and a needle insertion part. The positioning part consists of a construction for the placement of the whole robotic device relative to the prostate and an arch on which the insertion part is positioned. The main elements of the insertion part are a telescopic cylinder to move the whole tapping device forward after each tap and to set the needle insertion depth per tap, a tapping device to tap the needle in and out the prostate (Lagerburg *et al.*, 2006a), and a buffer stop to prevent the insertion depth to exceed the predefined distance.

Some first MRI compatibility tests were performed with this prototype robotic device. For this reason the robotic device was placed in a 1.5 T MRI scanner. First MR images were made to investigate whether the device caused image artefacts. Thereafter the working of the robotic device in a magnetic field was tested and compared with its working outside the scanner. The robotic device did not give any artefacts and the working inside the MRI scanner was not influenced by the magnetic field.

Meanwhile other research groups are also developing devices for MRI-guided interventions. Not only for prostate, but also for e.g. breast and cardiovascular interventions. Both Engelhard *et al.* (2006) and Beyersdorff *et al.* (2005) developed devices for transrectal prostate biopsy. The feasibility of the devices was shown in a patient study. Susil *et al.* (2003, 2004, 2006) developed a device that was suitable for several prostate interventions. In a canine study they showed the feasibility of the robotic device for transrectal prostate biopsy and brachytherapy (Susil *et al.*, 2003). In Susil *et al.* (2004) the feasibility of a system for transperineal HDR was shown in a patient study. Muntener *et al.* (2006) and Patriciu *et al.* (2007) developed a MRI compatible robot capable of automated brachytherapy seed placement. Some pre-clinical phantom experiments were performed to test needle and seed placement accuracy of the robotic device.

There are some major differences between the systems described in literature for transperineal MRI-guided brachytherapy and the robotic device developed at our department. With the system described in Susil *et al.* (2004) the patient has to be moved in and out the scanner for needle insertion and imaging. After the needles are positioned the patient is moved to a shielded room for the HDR treatment. With the system we developed the patient stays in the scanner during the whole procedure as in the system described by Muntener *et al.* (2006). With both systems from literature the patient is placed in the left lateral decubitus position. A major concern with this position for a longer period is the stability of the patient and the potential for brachial plexopathy and injuries to cutaneous pressure points. With the use of our robotic device the patient is positioned in the supine position with his knees slightly bent to provide the necessary space. In a feasibility study we showed that with this method we are able to cover the prostate with the prescribed dose without piercing the urethra or rectum and without pubic bone interference (Van Gellekom *et al.*, 2004). Another major difference is the needle insertion method. In the systems described in literature the needle is pushed into the prostate, while with our system the needle is tapped into the prostate. In Lagerburg *et al.* (2006b) we showed that prostate motion is significant reduced with this new needle insertion method. This makes it possible to accurately deposit the seeds and achieve the planned dose distribution.

In conclusion, at this moment prostate brachytherapy is performed under ultrasound-guidance. To improve the dose distribution a better image quality is of importance which is offered by MRI. Due to the limited amount of space inside a closed bore scanner a robotic device is necessary. One of the main causes of seed misplacement during the procedure is prostate motion. Therefore this robotic device is equipped with a tapping device which diminishes prostate motion during needle insertion. This tapping device taps the needle into the prostate, instead of the currently used method of pushing the needle. When this is done with a high velocity, the prostate motion will decrease. In a clinical study the effectiveness of this tapping device was demonstrated. MRI compatibility tests of the robotic device in a 1.5 T MRI scanner showed its proper working in a magnetic field without causing image artefacts. In the near future preclinical experiments will be performed to test the functionality, and the needle and seed placement accuracy of the robotic device. Thanks to the MRI-guided new needle insertion method we think that more accurate seed placement,

boosting of tumour volume, and sparing of critical structures is possible, in order to further optimise prostate dose distributions. Besides for LDR and HDR prostate brachytherapy this robotic device can also be useful in other applications where tissue motion due to needle insertion is problematic, such as prostate and breast biopsies (Deurloo *et al.*, 2001).

Samenvatting

Jaarlijks wordt er in Nederland bij ruim 7000 mannen prostaatkanker vastgesteld. Afhankelijk van het stadium van de ziekte en de conditie van de patiënt zijn er verschillende behandelmethoden mogelijk. Bij de kleinere, niet uitgezaaide tumoren zijn er drie gebruikelijke behandelmethoden: prostatectomie, uitwendige bestraling en inwendige bestraling. Bij een prostatectomie wordt de gehele prostaat chirurgisch verwijderd, bij uitwendige bestraling wordt de prostaat gedurende een aantal weken van buitenaf bestraald en bij inwendige bestraling worden er radioactieve bronnen achtergelaten in de prostaat. Vaak worden hiervoor jodium-125 bronnen, ook wel zaadjes genoemd, gebruikt. Het voordeel van deze laatste methode is dat de omringende weefsels minder straling krijgen, doordat de dosis snel afneemt buiten de zaadjes. Bij deze methode is het heel belangrijk dat de zaadjes op de goede plek terechtkomen, omdat een afwijking van de positie van de zaadjes ten opzichte van de geplande positie een grote invloed kan hebben op de dosisverdeling. Om de zaadjes goed neer te kunnen leggen is visualisatie van de prostaat van belang. Momenteel wordt de implantatieprocedure uitgevoerd onder ultrasound (US) geleide. Hiermee is de prostaat niet altijd even goed af te beelden. Met behulp van MRI (Magnetic Resonance Imaging) is de prostaat duidelijker te zien en zijn er ook structuren binnen de prostaat zichtbaar. Met behulp van nieuwe technieken zoals MR spectroscopie, perfusie-gewogen MRI en diffusie-gewogen MRI wordt het zelfs mogelijk om de tumor binnen de prostaat te zien. Hierdoor kan er extra dosis gegeven worden aan de tumor. MRI heeft echter twee grote nadelen: de beperkte ruimte binnen de conventionele, gesloten, MRI scanners en de aantrekkingskracht van het magnetische veld op de chirurgische instrumenten. De huidige implantatiemethode, waarbij de patiënt in de lithotomie positie ligt en een template gebruikt wordt voor het geleiden van de naalden, is vanwege

de beperkte ruimte in de MRI niet te gebruiken. Het is daarom noodzakelijk om deze methode aan te passen. Het handmatig inbrengen van de naalden en vervolgens met MRI afbeelden is mogelijk, maar dan moet de patiënt tijdens de procedure vele malen in en uit de scanner geschoven worden. Met het gebruik van een robot die in de MRI scanner tussen de benen van de patiënt past, is dit probleem opgelost. Bij het ontwerpen van de robot zal er bij de materiaalkeuze wel rekening gehouden moeten worden met het magnetische veld in de MRI scanner. In dit proefschrift worden de eerste stappen in de ontwikkeling van een robot voor prostaat brachytherapie onder MRI-geleide beschreven.

De robot maakt gebruik van een nieuwe implantatiemethode, de *single needle implant method*. Met deze methode wordt tijdens de gehele procedure maar één naald gebruikt. Deze naald wordt in de prostaat gebracht, door een rotatiepunt dat vlak onder de huid gekozen wordt. Nadat de zaadjes ingebracht zijn, wordt de naald teruggetrokken tot aan het rotatiepunt, waarna de naald weer onder een andere hoek ingebracht kan worden. Dit in tegenstelling tot de huidige methode waarbij eerst alle naalden, parallel aan elkaar, ingebracht worden en dan pas de zaadjes achtergelaten worden. Met de nieuwe implantatiemethode wordt er geen gebruik gemaakt van een template of van *locking needles*. Een bijkomend voordeel van deze methode zou kunnen zijn dat er minder trauma ontstaat bij het perineum doordat er maar één intreepunt in de huid is.

Een van de oorzaken van afwijkingen in de positie van de jodiumzaadjes ten opzichte van de geplande positie is prostaatbeweging. Omdat een afwijking van de zaadpositie ten opzichte van de geplande positie een significante invloed kan hebben op de dosisverdeling in de prostaat, is het van belang te weten hoe(veel) de prostaat beweegt tijdens het inbrengen van de naald. Voor de ontwikkeling van de robot is dit nog belangrijker omdat de nieuwe implantatie-methode gevoeliger is voor prostaatbeweging dan de oude. In de oude methode worden eerst alle naalden in de prostaat gebracht voordat de zaadjes ingebracht worden, waardoor prostaatbeweging tussen het inbrengen van de verschillen-de zaadjes minimaal is. Bij de nieuwe methode is iedere keer dat de naald ingebracht wordt prostaatbeweging mogelijk.

In hoofdstuk 2 hebben we onderzoek gedaan naar prostaatrotatie ten gevolge van het inbrengen van de naald. We hebben hierbij gekeken naar de prostaat-rotatie in twee vlakken, het coronale vlak en het sagittale vlak.

In veel instituten wordt gebruikt gemaakt van zogenaamde *locking needles* om

de prostaatbeweging te verminderen. In de literatuur bestaat weinig duidelijkheid over het nut van deze naalden. Tijdens ons onderzoek hebben we daarom ook gekeken naar de invloed van de *locking needles* op de prostaatrotatie. De rotatie werd gemeten door een 3D scan te maken nadat de naald in de prostaat was ingebracht en daarna nog een 3D scan als de naald uit de prostaat was gehaald en de zaadjes achtergelaten waren. Het verschil in oriëntatie tussen de naald en de zaadjes is de prostaatrotatie. In het coronale vlak verminderden de *locking needles* de rotatie significant van 13.8 graden zonder naar 7.8 graden met *locking needles*. In het sagittale vlak hadden de *locking needles* geen invloed op de prostaatrotatie. Een prostaatrotatie van 13.8 graden kan een fout in de positie van het zaadje opleveren van 8.4 mm als een *strand* van vier zaadjes gebruikt wordt. Vooral in het sagittale vlak bleek de prostaatrotatie onafhankelijk te zijn van de plek waar de naald in de prostaat gestoken werd. Het is dus niet mogelijk om met het plannen van de posities van de zaadjes rekening te houden met de prostaatrotatie en daarom zal er een andere oplossing gevonden moeten worden om de zaadjes nauwkeurig neer te leggen.

Een mogelijke oplossing is het verminderen van de prostaatbeweging tijdens het inbrengen van de naald door deze met hoge snelheid en bekende impuls naar binnen te tikken in plaats van de huidige methode waarbij de naald naar binnen geduwd wordt. Door de hoge snelheid verwachten we minder prostaatbeweging.

In hoofdstuk 3 wordt de ontwikkeling beschreven van een slagmechanisme waarmee de naalden tijdens de implantatie naar binnen getikt kunnen worden. Eerst is er tijdens een gewone implantatieprocedure gemeten hoeveel impuls er nodig is om een naald naar binnen te tikken. Hiervoor is een drukgevoelige sensor (Flexiforce A201, Tekscan) bevestigd op het uiteinde van de naald en vervolgens heeft een arts de naald handmatig naar binnen getikt. De gemeten impuls varieerde van 0.13 ± 0.02 Ns tot 1.16 ± 0.15 Ns met een gemiddelde impuls van 0.50 ± 0.07 Ns. De grote spreiding in impuls correspondeerde met een grote spreiding in de afstand die de naald de prostaat in gebracht werd per slag (4.25 mm tot 17.5 mm met een gemiddelde van 7.9 mm). De gemeten impuls is daarna gebruikt als referentie voor het te maken slagmechanisme.

We hebben gekozen voor een impuls gedreven systeem omdat dit inherent veiliger is dan een kracht gedreven systeem. Als de naald bijvoorbeeld een botachtige structuur raakt dan zal de naald zijn impuls overbrengen en dan stoppen met bewegen, terwijl in een kracht gedreven systeem de naald de botachtige

structuur zal binnendringen.

De belangrijkste onderdelen van het slagmechanisme zijn een pneumatische cilinder, een bewegend blokje en een stootblok. De pneumatische cilinder beweegt onder druk vooruit en duwt het blokje voort. Als de cilinder zijn maximale slag (4 cm) heeft bereikt, beweegt het blokje verder met een constante snelheid. Dit blokje raakt vervolgens de naald, waardoor de naald in de prostaat getikt wordt. De afstand die de naald per slag de prostaat in gaat is instelbaar met behulp van het stootblok. De maximale snelheid van de pneumatische cilinder en dus de snelheid waarmee de naald de prostaat binnengaat is instelbaar met behulp van de luchtdruk op de pneumatische cilinder en hangt ook af van het gewicht van het blokje. De werking van het slagmechanisme is getest op een stuk vlees dat op een vrij draaibaar en beweegbaar plateau geplaatst was. Tijdens de tests bleek dat met toenemende druk op de pneumatische cilinder, en dus hogere snelheid van het blokje, de verplaatsing van het vlees minder werd. Met een druk van 4 bar (de maximale druk haalbaar met deze opstelling, wat correspondeert met een impuls van 0.37 Ns) bewoog het vlees maximaal 2 mm en was de rotatie maximaal 6 graden. We verwachten dat met een hogere druk deze verplaatsing nog verder afneemt.

Na het testen van het slagmechanisme op een stuk vlees is tijdens een klinische studie, beschreven in hoofdstuk 4, gekeken naar het verschil in prostaatbeweging tussen het naar binnen duwen van de naald (de huidige methode) en het naar binnen tikken met behulp van het slagmechanisme. Hiervoor is het slagmechanisme zodanig aangepast dat het op de ultrasound stepper geplaatst kon worden.

Voor het meten van de prostaatbeweging zijn de ultrasound beelden van de implantatieprocedure opgenomen met behulp van een videorecorder. De prostaatbeweging is gedefinieerd als het verschil in prostaatpositie voor het naar binnenbrengen van de naald en nadat de naald op zijn uiteindelijke positie is aangekomen. De gemiddelde prostaatbeweging was significant minder als de naald naar binnen getikt werd in plaats van geduwd (5.6 mm (bereik 0.3 - 21.6) ten opzichte van 0.9 mm (bereik 0 - 2.0)). Voor de eerste vijf patiënten werd een druk van 6 bar gebruikt. Dit komt overeen met een impuls van 0.49 ± 0.06 Ns, wat gelijk is aan de gemiddelde impuls die de arts nodig had om een naald naar binnen te tikken. Omdat bij sommige patiënten de naald niet de vooraf gedefinieerde afstand van 5 mm per slag de prostaat in ging, is na de eerste

paar patiënten de druk verhoogd naar 8 bar (dit correspondeert met een impuls van 0.61 ± 0.08 Ns). Hierdoor verminderde de gemiddelde prostaatbeweging van 1.4 mm naar 0.7 mm. We verwachten dat met een hogere druk, de prostaatbeweging nog verder afneemt.

Om de jodiumzaadjes op de geplande positie neer te leggen is een goed beeld van de prostaat, de naald en de zaadjes nodig. MRI geeft een goed contrast tussen zachte weefsels, wat het mogelijk maakt om structuren in de prostaat te definiëren. Een nadeel van MRI is de noodzakelijkheid om de normaal gebruikte methode en materialen aan te passen vanwege de beperkte ruimte in de MRI en de aantrekkingskracht van het magneetveld op de gebruikte materialen. De enige momenteel commercieel verkrijgbare MRI compatibele naalden zijn gemaakt van titanium. Dit materiaal geeft nog steeds een verstoring van het MRI beeld, vooral bij de tip van de naald. Een naald met een diameter van 1.3 mm, de buitenmaat van de normaal gebruikte brachytherapie naalden, geeft een artefact aan de tip van de naald van ongeveer 4 mm als de naald parallel aan het magneetveld is geplaatst. Dit maakt het moeilijk om de exacte positie van de zaadjes te bepalen (afmetingen 4.5 x 0.8 mm), hetgeen van belang is voor het bereiken van een nauwkeurige dosisverdeling in de prostaat.

In hoofdstuk 5 is onderzocht hoe het artefact van een jodiumzaadje eruit ziet en wat de invloed van verschillende naaldmaterialen op het artefact van een jodiumzaadje is, als het direct achter de tip van de naald geplaatst is. De naald is onder verschillende hoeken ten opzichte van het magnetisch veld gelegd, aangezien dit ook gebeurt tijdens de implantatie procedure. We hebben gebruik gemaakt van simulaties om de artefacten te bestuderen. Verder hebben we van een jodiumzaadje en van een titaniumnaald ook MRI scans gemaakt om te kunnen vergelijken met de simulaties. Eerst zijn de grootte en de positie van het artefact van het zaadje alleen geanalyseerd. Daarna is gekeken naar de invloed van de aanwezigheid van het naaldartefact op het zaadartefact. Dit is gedaan door de afstand tussen het einde van de echte positie van het zaadje en het einde van het artefact van het zaadje te meten. Als deze afstand verandert door de aanwezigheid van de naald, wordt het moeilijker om aan de hand van het artefact de exacte positie van het zaadje te bepalen.

De simulaties kwamen goed overeen met de simulaties uit de literatuur. De gemaakte MRI scans verschilden enigszins met de simulaties, maar de algehele vorm kwam overeen. De afstand van het einde van het artefact tot het

eind van het zaadje varieerde niet voor de onderzochte hoeken. De afstand hangt wel af van het naaldmateriaal dat gebruikt wordt en wordt kleiner als de susceptibiliteit van het materiaal dichter bij dat van menselijk weefsel (-9.0) komt. Alhoewel aluminium een susceptibiliteit van maar 20.7 heeft (in vergelijking met titanium met een susceptibiliteit van 182) wordt het artefact van het zaadje nog steeds beïnvloed door het artefact van de naald waardoor het moeilijk is om de exacte positie van het zaadje te bepalen op grond van de positie van het artefact. Uit de simulaties bleek dat het artefact van de tip van de titanium naald zodanig groot is, dat het artefact van het zaadje overschaduwd wordt. Alleen met een plastic naald is het artefact van het zaadje goed te onderscheiden van het artefact van de naald. Alhoewel een Gradient Echo (GE) sequentie een groter artefact geeft dan een Spin Echo (SE) sequentie is met een GE sequentie de zaadpositie nauwkeuriger te bepalen, omdat het midden van het zaadartefact goed overeen komt met het midden van de echte zaadpositie. Dit geeft een afwijking van minder dan 0.4 mm voor de scanparameters die we tijdens de simulatiestudie hebben gebruikt.

In hoofdstuk 6 wordt het eerste prototype robot voor prostaat brachytherapie onder MRI-geleide beschreven. Deze robot bestaat uit twee belangrijke delen: een deel voor het positioneren van de gehele robot en een deel voor het naar binnen tikken van de naald. Het positioneringsgedeelte bestaat ook weer uit twee delen: een gedeelte om aan het begin van de procedure de robot in de juiste positie te zetten zodat de naald zich recht voor het rotatiepunt bevindt en een boog om de naald in verschillende hoeken ten opzichte van het rotatiepunt te zetten. De belangrijkste onderdelen van het tikkende gedeelte zijn de telescoopcilinder en het slagmechanisme. De telescoopcilinder beweegt het slagmechanisme na iedere slag naar voren tijdens het naar binnen tikken van de naald en naar achteren tijdens het naar buiten tikken van de naald en wordt gebruikt om de slagdiepte in te stellen. Een bufferstop voorkomt dat de ingestelde slagdiepte overschreden wordt. Het slagmechanisme tikt de naald naar binnen en naar buiten en is gebaseerd op het principe beschreven in hoofdstuk 3.

Enkele MRI compatibiliteitstesten zijn uitgevoerd om de werking van de robot in een magneetveld te bestuderen. Hiervoor is de robot in een 1.5T MRI scanner geplaatst. Eerst zijn er enkele MR plaatjes gemaakt om te onderzoeken of de robot beeldartefacten veroorzaakt. Daarna is de werking van de robot in een

magneetveld getest en vergeleken met de werking buiten de scanner. Uit de testen bleek dat de robot geen artefacten in het beeld veroorzaakt en goed werkt in een magneetveld. Op korte termijn verwachten we de eerste pre-klinische testen te doen om de functionaliteit en de positioneringsnauwkeurigheid van de robot te testen.

Dankzij de nieuwe methode om de naalden in te brengen (tikken in plaats van duwen) en de nieuwe afbeeldingstechniek (MRI in plaats van US) denken we dat we de zaadjes nauwkeuriger in kunnen brengen dan met de huidige methode en de dosisverdeling beter kunnen afstemmen op de verdeling van tumorvolumes in de prostaat.

References

Alterovitz R, Goldberg K, Pouliot J, Taschereau R and Hsu I J 2003a Needle insertion and radioactive seed implantation in human tissues: simulation and sensitivity analysis in *IEEE International Conference on Robotics and Automation* pp. 1793–1799

Alterovitz R, Pouliot J, Taschereau R, Hsu I J and Goldberg K 2003b Simulating needle insertion and radioactive seed implantation for prostate brachytherapy in *Medicine Meets Virtual Reality* pp. 19–25

Bakker C J G, Bhagwandien R, Moerland M A and Ramos L M P 1994 Simulation of susceptibility artifacts in 2D and 3D Fourier transform spin-echo and gradient-echo magnetic resonance imaging *Magn. Res. Imaging* **12** 767–774

Balter J M, Lam K L, Sandler H M, Littles J F, Bree R L and Ten Haken R K 1995a Automated localization of the prostate at the time of treatment using implanted radiopaque markers: technical feasibility *Int. J. Radiat. Oncol. Biol. Phys.* **33** 1281–1286

Balter J M, Sandler H M, Lam K, Bree R L, Lichter A S and Ten Haken R K 1995b Measurement of prostate movement over the course of routine radiotherapy using implanted markers *Int. J. Radiat. Oncol. Biol. Phys.* **31** 113–118

Battermann J J 2000 I-125 implantation for localized prostate cancer: the Utrecht University experience *Radiother. Oncol.* **57** 269–272

Bernard S and Vynckier S 2005 Dosimetric study of a new polymer encapsulated palladium-103 seed *PMB* **50** 1493–1504

Beyersdorff D, Taupitz M, Winkelmann B, Fischer T, Lenk S, Loening S A and Hamm B 2002 Patients with a history of elevated prostate-specific antigen levels and negative transrectal US-guided quadrant or sextant biopsy results: value of MR imaging *Radiology* **224** 701–706

Beyersdorff D, Winkel A, Hamm B, Lenk S, Loening S A and Taupitz M 2005 MR imaging-guided prostate biopsy with a closed MR unit at 1.5T: Initial results *Radiology* **234** 576–581

Bhagwandien R, Moerland M A, Bakker C J G, Beersma R and Lagendijk J J W 1994

Numerical analysis of the magnetic field for arbitrary magnetic susceptibility distributions in 3D *Magn. Res. Imaging* **12** 101–107

Bhagwandien R, van Ee R, Beersma R, Bakker C J G, Moerland M A and Lagendijk J J W 1992 Numerical analysis of the magnetic field for arbitrary magnetic susceptibility distributions in 2D *Magn. Res. Imaging* **10** 299–313

Bolla M, Collette L, Blank L, Warde P, Dubois J B, Mirimanoff R O, Storme G, Bernier J, Kuten A, Sternberg C, Mattelaer J, Torecilla J L, Pfeffer J R, Cutajar C L, Zurlo A and Pierart M 2002 Long-term results with immediate androgen suppression and external irradiation in patients with locally advanced prostate cancer (an EORTC study): a phase III randomised trial *The Lancet* **360** 103–108

Buckley D L, Roberts C, Parker G J M, Logue J P and Hutchinson C E 2004 Prostate cancer: evaluation of vascular characteristics with dynamic contrast-enhanced T1-weighted MR imaging – initial experience *Radiol.* **233** 709–715

Chen M E, Johnston D A, Tang K, Babaian R J and P Troncoso 2000 Detailed mapping of prostate carcinoma foci - biopsy strategy implications *Cancer* **89** 1800–1809

Cheng D and Tempany C M C 1998 MR imaging of the prostate and bladder *Seminars in Ultrasound, CT, and MRI* **19** 67–89

Crook J M, Raymond Y, Salhani D, Yang H and Esche B 1995 Prostate motion during standard radiotherapy as assessed by fiducial markers *Radiother. Oncol.* **37** 35–42

Damber J-E and Khatami A 2005 Surgical treatment of localized prostate cancer *Acta Oncologica* **44** 599–604

D'Amico A V, Cormack R, Tempany C M, Kumar S, Topulos G, Kooy H M and Coleman C N 1998 Real-time magnetic resonance image-guided interstitial brachytherapy in the treatment of select patients with clinically localized prostate cancer *Int. J. Radiat. Oncol. Biol. Phys.* **42** 507–515

Dattoli M and Waller K 1997 A simple method to stabilize the prostate during transperineal prostate brachytherapy *Int. J. Radiat. Oncol. Biol. Phys.* **38** 341–342

Dawson J E, Wu T, Roy T, Gu J Y and Kim H 1994 Dose effects of seeds placement deviations from pre-planned positions in ultrasound guided prostate implants *Radiotherapy and Oncology* **32** 268–270

De Meerleer G, Villeirs G, Bral S, Paelinck L, De Gersem W, Dekuyper P and De Neve W 2005 The magnetic resonance detected intraprostatic lesion in prostate cancer: planning and delivery of intensity-modulated radiotherapy *Radiother. Oncol.* **75** 325–333

Dehnad H, Nederveen A J, Van der Heide U A, Van Moorselaar R J A, Hofman P and Lagendijk J J W 2003 Clinical feasibility study for the use of implanted gold seeds in the

prostate as reliable positioning markers during megavoltage irradiation *Radiother. Oncol.* **67** 295–302

Deurloo E E, Gilhuijs K G A, Schultze Kool L J and Muller S H 2001 Displacement of breast tissue and needle deviations during stereotactic procedures. *Investigative Radiology* **36** 347–353

DiMaio S P and Salcudean S E 2002a Needle insertion modelling and simulation in *IEEE International Conference on Robotics and Automation* pp. 2098–2105

DiMaio S P and Salcudean S E 2002b Needle insertion modelling for the interactive simulation of percutaneous procedures in *Medical Image Computation and Computer-Assisted Intervention* pp. 253–260

Efron B and Tibshirani R J 1993 *An introduction to the bootstrap* (Chapman & Hall)

Engelbrecht M R, Jager G J, Laheij R J, Verbeek A L M, Van Lier H J and Barentsz J O 2002 Local staging of prostate cancer using magnetic resonance imaging: a meta-analysis *European Radiology* **12** 2294–2302

Engelhard K, Hollenbach H P, Kiefer B, Winkel A, Goeb K and Engehausen D 2006 Prostate biopsy in the supine position in a standard 1.5-T scanner under real time MR-imaging control using a MR-compatible endorectal biopsy device *European Radiology* **16** 1237–1243

Engelhard K, Hollenbach H P, Riedle Ch, Ott G, Hausmann J and Risse W 2001 Magnetic resonance imaging as an aid in helping the physician diagnose benign prostatic disease and prostatic carcinoma *Electromedica* **69** 38–43

Feygelman V, Friedland J L, Sanders R M, Noriega B K and Pow-Sang J M 1996 Improvement in dosimetry of ultrasound-guided prostate implants with the use of multiple stabilization needles *Medical Dosimetry* **21** 109–112

Fichtinger G, Burdette E C, Tanacs A, Patriciu A, Mazilu D, Whitcomb L L and Stoianovici D 2006 Robotically assisted prostate brachytherapy with transrectal ultrasound guidance - phantom experiments *Brachytherapy* **5** 14–26

Fichtinger G, DeWeese T L, Patriciu A, Tanacs A, Mazilu D, Anderson J H, Masamune K, Taylor R H and Stoianovici D 2002a System for robotically assisted prostate biopsy and therapy with intraoperative CT guidance *Academic Radiology* **9** 60–74

Fichtinger G, Krieger A, Susil R C, Tanacs A, Whitcomb L L and Atalar E 2002b Transrectal prostate biopsy inside closed MRI scanner with remote actuation, under real-time image guidance in *Proceedings of the fifth international conference on Medical Image Computing and Computer Assisted Intervention, Lecture notes in computer science 2488, Part 1* pp. 91–98

Gerbaulet A, Pötter R, Mazeron J, Meertens H and Van Limbergen E 2002 *The GEC ESTRO handbook of brachytherapy* (Leuven, Be: ESTRO)

Haider M A, van der Kwast T H, Tanguay J, Evans A J, Hashmi A T, Lockwood G and Trachtenberg J 2007 Combined t2-weighted and diffusion-weighted MRI for localization of prostate cancer *American Journal of Roentgenology* **189** 323–328

Harris S J, Arambula-Cosio F, Mei Q, Hibberd R D, Davies B L, Wickham J E, Nathan M S and Kundu B 1997 The probot - an active robot for prostate resection in *Proceedings of the Institution of Mechanical Engineers. Part H, Journal of Engineering in Medicine* vol. 211 pp. 317–325

Holm H H, Juul N, Pedersen J F, Hansen H and Strøyer I 1983 Transperineal ^{125}iodine seed implantation in prostatic cancer guided by transrectal ultrasonography *J. Urol.* **130** 283–286

Holton L L H 2001 Force models for needle insertion created from measured needle puncture data *Studies in health technology and informatics* **81** 180–186

Hsu C Y, Joniau S, Oyen R, Roskams T and Van Poppel H 2006 Detection of clinical unilateral T3a prostate cancer - by digital rectal examination or transrectal ultrasonography? *BJU International* **98** 982–985

Husband J E, Padhani A R, MacVicar A D and Revell P 1998 Magnetic resonance imaging of prostate cancer: comparison of image quality using endorectal and pelvic phased array coils *Clin. Radiol.* **53** 673–681

Kaplan I D, Meskell P M, Lieberfarb M, Saltzman B, Berg S and Holupka E J 2004 A comparison of the precision of seeds deposited as loose seeds versus suture embedded seeds: a randomized trial *Brachytherapy* **3** 7–9

Karaiskos P, Papagiannis P, Sakelliou L, Anagnostopoulos G and Baltas D 2001 Monte Carlo dosimetry of the selectseed ^{125}I interstitial brachytherapy seed *Medical Physics* **28** 1753–1760

Kataoka H, Washio T, Chinzei K, Mizuhara K, Simone C and Okamura A M 2002 Measurement of the tip and friction force acting on a needle during penetration in *Proceedings of the fifth international conference on medical image computing and computer assisted intervention* pp. 216–223

Khoo V S 2005 Radiotherapeutic techniques for prostate cancer, dose escalation and brachytherapy *Clinical Oncology* **17** 560–571

Konings M K, Bartels L W, Smits H F M and Bakker C J G 2000 Heating around intravascular guidewires by resonating RF waves *Journal of Magnetic Resonance Imaging* **12** 79–85

Krieger A, Susil R C, Ménard C, Coleman J A, Fichtinger G, Atalar E and Whitcomb L L 2005

Design of a novel MRI compatible manipulator for image guided prostate interventions *IEEE Transactions on biomedical engineering* **52** 306–313

Kuban D A, Tucker S L, Dong L, Starkschall G, Huang E H, Cheung M R, Lee A K and Pollack A 2008 Long-term results of the M.D.Anderson randomized dose-escalation trial for prostate cancer *Int. J. Radiat. Oncol. Biol. Phys.* **70** 67–74

Kupelian P A, Potters L, Khuntia D, Ciezki J P, Reddy C A, Reuther A M, Carlson T P and Klein E A 2004 Radical prostatectomy, external beam radiotherapy <72 Gy, external beam radiotherapy ≥72 Gy, permanent seed implantation, or combined seeds/external beam radiotherapy for stage T1-T2 prostate cancer *Int. J. Radiat. Oncol. Biol. Phys.* **58** 25–33

Lagendijk J J W, Bartels L W, Dehnad H, Van Vulpen M, Van der Heide U A, Ceylan C, Seppenwoolde J H, Tersteeg J H A and Raaymakers B W 2004 MRI-based treatment planning for prostate tumours: fiducial marker-based registration and position verification in *International conference on the Use of Computers in Radiation Therapy* pp. 93–95

Lagendijk J J W, Raaymakers B W, Raaijmakers A J E, Overweg J, Brown K J, Kerkhof E M, van der Put R W, Hårdemark B, van Vulpen M and van der Heide U A 2008 MRI/linac integration *Radiother. Oncol.* **86** 25–29

Lagerburg V, Moerland M A, Konings M K, Van de Vosse R E, Lagendijk J J W and Battermann J J 2006a Development of a tapping device: a new needle insertion method for prostate brachytherapy *Phys. Med. Biol.* **51** 891–902

Lagerburg V, Moerland M A, Lagendijk J J W and Battermann J J 2005 Measurement of prostate rotation during insertion of needles for brachytherapy *Radiother. Oncol.* **77** 318–323

Lagerburg V, Moerland M A, Van Vulpen M and Lagendijk J J 2006b A new robotic needle insertion method to minimise attendant prostate motion *Radiotherapy and Oncology* **80** 73–77

Lefrançois R and Sloboda R S 2003 A medical needle drive for the study of interstitial implant mechanics. *Medical Engineering & Physics* **25** 255–258

Lu-Yao G L and Yao S L 1997 Population-based study of long-term survival in patients with clinically localised prostate cancer *The Lancet* **349** 906–910

Mahnken A H, Chalabi K, Jalali F, Günther R and Buecker A 2004 Magnetic resonance-guided placement of aortic stents grafts: feasibility with real-time magnetic resonance fluoroscopy *Journal of vascular and interventional radiology* **15** 189–195

Mangar S A, Huddart R A, Parker C C, Dearnaley D P, Khoo V S and Horwich A 2005 Technological advances in radiotherapy for the treatment of localised prostate cancer *European Journal of Cancer* **41** 908–921

Maurin B, Barbe L, Bayle B, Zanne P, Gangloff J, De Mathelin M, Gangi A, Soler L and Forgione A 2004 In vivo study of forces during needle insertions in *Proceedings of the Medical Robotics, Navigation and Visualisation Scientific Workshop*

McLaughlin P W, Troyer S, Berri S, Narayana V, Meirowitz A, Roberson P L and Montie J 2005 Functional anatomy of the prostate: implications for treatment planning *Int. J. Radiat. Oncol. Biol. Phys.* **63** 479–491

Ménard C, Susil R C, Choyke P, Gustafson G S, Kammerer W, Ning H, Miller R W, Ullman K L, Sears Crouse N, Smith S, Lessard E, Pouliot J, Wright V, McVeigh E, Coleman C N and Camphausen K 2004 MRI-guided HDR prostate brachytherapy in standard 1.5T scanner *Int. J. Radiat. Oncol. Biol. Phys.* **59** 1414–1423

Merrick G S, Butler W M, Wallner K E, Galbreath R W and Lief J H 2003a Long-term urinary quality of life after permanent prostate brachytherapy *Int. J. Radiat. Oncol. Biol. Phys.* **56** 454–461

Merrick G S, Butler W M, Wallner K E, Hines A L and Allen Z 2003b Late rectal function after prostate brachytherapy *Int. J. Radiat. Oncol. Biol. Phys.* **57** 42–48

Merrick G S, Butler W M, Wallner K E, Lief J H, Anderson R L, Smeiles B J, Galbreath R W and Benson M L 2002 The importance of radiation doses to the penile bulb vs. crura in the development of postbrachytherapy erectile dysfunction *Int. J. Radiat. Oncol. Biol. Phys.* **54** 1055–1062

Merrick G S, Wallner K, Butler W M, Galbreath R W, Lief J H and Benson M L 2001 A comparison of radiation dose to the bulb of the penis in men with and without prostate brachytherapy-induced erectile dysfunction *Int. J. Radiat. Oncol. Biol. Phys.* **50** 597–604

Mikhail A A, Orvieto M A, Billatos E S, Zorn K C, Gong E M, Brendler C B, Zagaja G P and Shalhav A L 2006 Robotic-assisted laparoscopic prostatectomy: first 100 patients with one year of follow-up *Urology* **68** 1275–1279

Miller D C, Sanda M G, Dunn R L, Montie J E, Pimentel H, Sandler H M, McLaughlin W P and Wei J T 2005 Long-term outcomes among localized prostate cancer survivors: health-related quality-of-life changes after radical prostatectomy, external radiation, and brachytherapy *Journal of Clinical Oncology* **23** 2772–2780

Moerland M A, Wijrdeman H K, Beersma R, Bakker C J G and Battermann J J 1997 Evaluation of permanent I-125 prostate implants using radiography and magnetic resonance imaging *Int. J. Radiat. Oncol. Biol. Phys.* **37** 927–933

Müller-Bierl B, Graf H, Steidle G and Schick F 2005 Compensation of magnetic field distortions from paramagnetic instruments by added diamagnetic material: Measurements and numerical simulations *Medical Physics* **32** 76–84

Mullerad M, Hricak H, Kuroiwa K, Pucar D, Chen H, Kattan M W and Scardino P T

2005 Comparison of endorectal magnetic resonance imaging, guided prostate biopsy and digital rectal examination in the preoperative anatomical localization of prostate cancer *The Journal of Urology* **174** 2158–2163

Muntener M, Patriciu A, Petrisor D, Mazilu D, Bagga H, Kavoussi L, Cleary K and Stoianovici D 2006 Magnetic resonance imaging compatible robotic system for fully automated brachytherapy seed placement *Urology* **68** 1313–1317

Nath S, Chen Z, Yue N, Trumpore S and Peschel R 2000 Dosimetric effects of needle divergence in prostate seed implant using I-125 and Pd-103 radioactive seeds *Med. Phys.* **27** 1058–1066

Okamura A M, Simone C and O'Leary M D 2004 Force modeling for needle insertion into soft tissue *IEEE transactions on biomedical engineering* **51** 1707–1716

Paetzel C, Zorger N, Bachthaler M, Hamer O W, Stehr A, Feuerback S, Lenhart M, Völk M, Herold T, Kasprzak P and Nitz W R 2005 Magnetic resonance-guided percutaneous angioplasty of femoral and popliteal artery stenoses using real-time imaging and intra-arterial contrast-enhanced magnetic resonance angiography *Investigative radiology* **40** 257–262

Patriciu A, Petrisor D, Muntener M, Mazilu D, Schär M and Soianovici D 2007 Automatic brachytherapy seed placement under MRI guidance *IEEE Transactions on biomedical engineering* **54** 1499–1506

Peeters S T H, Heemsbergen W D, Koper P C M, Van Putten W L J, Slot A, Dielwart M F H, Bonfrer J M G, Incrocci L and Lebesque J V 2006 Dose-response in radiotherapy for localized prostate cancer: results of the Dutch multicenter randomized phase III trial comparing 68 Gy of radiotherapy with 78 Gy *J. Clin. Oncol.* **24** 1990–1996

Perlet C, Heywang-Kobrunner S H, Heinig A, Sittek H, Casselman J, Anderson I and Taourel P 2006 Magnetic resonance-guided, vacuum-assisted breast biopsy *Cancer* **106** 982–990

Peschel R E and Colberg J W 2003 Surgery, brachytherapy, and external beam radiotherapy for early prostate cancer *Lancet Oncol.* **4** 233–241

Podder T, Clark D, Sherman J, Fuller D, Messing E, Rubens D, Strang J, Brasacchio R, Liao L, Ng W-S and Yu Y 2006 In vivo motion and force measurement of surgical needle intervention during prostate brachytherapy *Medical Physics* **33** 2915–2922

Pollack A, Hanlon A L, Horwitz E M, Feigenberg S J, Konski A A, Movsas B, Greenberg R E, Uzzo R G, Ma C M C, McNeeley S W, Buyyounouski M K and Price R A 2006 Dosimetry and preliminary acute toxicity in the first 100 men treated for prostate cancer on a randomized hypofractionation dose escalation trial *Int. J. Radiat. Oncol. Biol. Phys.* **64** 518–526

Potters L, Klein E A, Kattan M W, Reddy C A, Ciezki J P, Reuther A M and Kupelian P A

2004 Monotherapy for stage T1-T2 prostate cancer: radical prostatectomy, external beam radiotherapy, or permanent seed implantation *Radiotherapy and Oncology* **71** 29–33

Raaymakers B W, Lagendijk J J W, Van der Heide U A, Overweg J, Brown K, Topolnjak R, Dehnad H, Jurgenliemk-Schulz I M, Welleweerd J and Bakker C J G 2004 Integrating a MRI scanner with a radiotherapy accelerator: a new concept of precise on line radiotherapy guidance and treatment monitoring in *The Use of Computers in Radiation Therapy*, eds. B Yong, S Do, E Kyung and W Sung pp. 89–92 ICCR Jeong Publishing

Raja J, Ramachandran N, Munneke G and Patel U 2006 Current status of transrectal ultrasound-guided prostate biopsy in the diagnosis of prostate cancer *Clinical Radiology* **61** 142–153

Rasch C, Barillot I, Remeijer P, Touw A, Van Herk M and Lebesque J V 1999 Definition of the prostate in CT and MRI: a multi-observer study *Int. J. Radiat. Oncol. Biol. Phys.* **43** 57–66

Reinsberg S A, Payne G S, Riches S F, Ashley S, Brewster J M, Morgan V A and deSouza N M 2007 Combined use of diffusion-weighted MRI and 1h MR spectroscopy to increase accuracy in prostate cancer detection *American Journal of Roentgenology* **188** 91–98

Remzi M, Dobrovits M, Reissigl A, Ravery V, Waldert M, Wiunig C, Fong Y K and Djavan B 2004 Can power doppler enhanced transrectal ultrasound guided biopsy improve prostate cancer detection on first and repeat prostate biopsy *European Urology* **46** 451–456

Roberson P L, Narayana V, McShan D L, Winfield R J and McLaughlin P W 1997 Source placement error for permanent implant of the prostate *Med. Phys.* **24** 251–257

Scheidler J, Hricak H, Vigneron D B, Yu K K, Sokolov D L, Huang L R, Zaloudek C J, Nelson S J, Carroll P R and Kurhanewicz J 1999 Prostate cancer: localization with three-dimensional proton MR spectroscopic imaging - clinicopathologic study *Radiology* **213** 473–480

Schneider C M, Okamura A M and Fichtinger G 2004 A robotic system for transrectal needle insertion into the prostate with integrated ultrasound in *Proceedings of the 2004 IEEE international conference on Robotics & Automation* pp. 365–370

Smitsmans M H P, De Bois J, Sonke J J, Betgen A, Zijp L J, Jaffray D A, Lebesque J V and Van Herk M. 2005 Automatic prostate localization on cone-beam CT scans for high precision image-guided radiotherapy *Int. J. Radiat. Oncol. Biol. Phys.* **63** 975–984

Sonnad S S, Langlotz C P and Schwartz J S 2001 Accuracy of MR imaging for staging prostate cancer: a meta-analysis to examine the effect of technologic change *Academic Radiology* **8** 149–157

Stone N N, Roy J, Hong S, Lo Y-C and Stock R G 2002 Prostate gland motion and deformation caused by needle placement during brachytherapy *Brachytherapy* **1** 154–160

Stone N N and Stock R G 2002 Complications following permanent prostate brachytherapy *European Urology* **41** 427–433

Susil R C, Camphausen K, Choyke P, McVeigh E R, Gustafson G S, Ning H, Miller R W, Atalar E, Coleman C N and Ménard C 2004 System for prostate brachytherapy and biopsy in a standard 1.5T MRI scanner *Magnetic Resonance in Medicine* **52** 683–687

Susil R C, Krieger A, Derbyshire J A, Tanacs A, L Withcomb L, Fichtinger G and Atalar E 2003 System for MR image-guided prostate interventions: canine study *Radiology* **228** 886–894

Susil R C, Ménard C, Krieger A, Coleman J A, Camphausen K, Choyke P, Fichtinger G, L Withcomb L, Coleman C N and Atalar E 2006 Transrectal prostate biopsy and fiducial marker placement in a standard 1.5T magnetic resonance imaging scanner *The journal of Urology* **175** 113–120

Taschereau R, Pouliot J, Roy J and Tremblay D 2000 Seed misplacement and stabilizing needles in transperineal permanent prostate implants *Radiother. Oncol.* **55** 59–63

Teillac P 2004 The global state of prostate cancer: new diagnostic tools, minimal requirements for diagnosis and staging, and guidelines in the second millennium *BJU International* **94** 3–4

Van der Heide U A, Kotte A N T J, Dehnad H, Hofman P, Lagendijk J J W and Van Vulpen M 2007 Analysis of fiducial marker-based position verification in the external beam radiotherapy of patients with prostate cancer *Radiotherapy and Oncology* **82** 38–45

Van Gellekom M P R, Moerland M A, Battermann J J and Lagendijk J J W 2004 MRI-guided prostate brachytherapy with single needle method-a planning study *Radiother. Oncol.* **71** 327–332

Van Herk M, Bruce A, Kroes A P G, Shouman T, Touw A and Lebesque J V 1995 Quantification of organ motion during conformal radiotherapy of the prostate by three dimensional image registration *Int. J. Radiat. Oncol. Biol. Phys.* **33** 1311–1320

Vicini F A, Kini V R, Edmundson G, Gustafson G S, Stromberg J and Martinez A 1999 A comprehensive review of prostate cancer brachytherapy: defining an optimal technique *Int. J. Radiat. Oncol. Biol. Phys.* **44** 483–491

Villeirs G M, Van Vaerenbergh K, Vakaet L, Bral S, Claus F, De Neve W J, Verstraete K L and De Meerleer G O 2005a Interobserver delineation variation using CT versus combined CT + MRI in intensity-modulated radiotherapy for prostate cancer *Strahlenther. Onkol.* **181** 424–430

Villeirs G M, Verstraete K L, De Neve W J and De Meerleer G O 2005b Magnetic resonance imaging anatomy of the prostate and periprostatic area: a guide for radiotherapists. *Radiother. Oncol.* **76** 99–106

Wachowicz K, Thomas S D and Fallone B G 2006 Characterization of the susceptibility artifact around a prostate brachytherapy seed in MRI *Medical Physics* **33** 4459–4467

Wefer A E, Hricak H, Vigneron D B, Coackley F V, Lu Y, Wefer J, Mueller-Lisse U, Carroll P R and Kurhanewicz J 2000 Sextant localization of prostate cancer: comparison of sextant biopsy, magnetic resonance imaging and magnetic resonance spectroscopy imaging with step section histology *The Journal of Urology* **164** 400–404

Wei J T, Dunn R L, Sandler H M, McLaughlin W, Montie J E, Litwin M S, Nyquist L and Sanda M G 2002 Comprehensive comparison of health-related quality of life after contemporary therapies for localized prostate cancer *Journal of Clinical Oncology* **20** 557–566

Weldon V E 2002 Technique of modern radical perineal prostatectomy *Urology* **60** 689–694

Yang M and Zahn J D 2004 Microneedle insertion force reduction using vibratory actuation *Biomedical Microdevices* **6** 177–182

Yu K K, Hricak H, Alagappan R, Chernoff D M, Bacchetti P and Zaloudek C J 1997 Detection of extracapsular extension of prostate carcinoma with endorectal and phased-array coil MR imaging: multivariate feature analysis *Radiology* **202** 697–702

Yu Y, Podder T, Zhang Y, Ng W-S, Misic V, Sherman J, Fu L, Fuller D, Messing E, Rubens D, Strand J and Brasacchio R 2006 Robot-assisted prostate brachytherapy in *Proceedings of the ninth international conference on Medical Image Computing and Computer Assisted Intervention, Lecture notes in computer science* pp. 41–49

Zelefsky M J, Yamada Y, Cohen G N, Shippy A, Chan H, Fridman D and Zaider M 2007 Five-year outcome of intraoperative conformal permanent I-125 interstitial implantation for patients with clinically localized prostate cancer *Int. J. Radiat. Oncol. Biol. Phys.* **67** 65–70

Publications

- Van Putten M J, Kind T, Visser F, Lagerburg V 2005 Detecting temporal lobe seizures from scalp EEG recordings: a comparison of various features *Clinical neurophysiology* **116** 2480–2489
- Lagerburg V, Moerland M A, Lagendijk J J W, Battermann J J 2005 Measurement of prostate rotation during insertion of needles for brachytherapy *Radiotherapy and Oncology* **77** 318–323
- Lagerburg V, Moerland M A, Konings M K, van de Vosse R E, Lagendijk J J W, Battermann J J 2006 Development of a tapping device: a new needle insertion method for prostate brachytherapy *Physics in Medicine and Biology* **51** 891–902
- Lagerburg V, Moerland M A, van Vulpen M, Lagendijk J J W 2006 A new robotic needle insertion method to minimise attendant prostate motion *Radiotherapy and Oncology* **80** 73–77
- Lagerburg V, Moerland M A, Seppenwoolde J H, Lagendijk J J W 2008 Simulation of the artefact of an iodine seed placed at the needle tip in MRI-guided prostate brachytherapy *Physics in Medicine and Biology* **53** N59-N67

Dankwoord

Na ruim vier jaar met veel plezier op de afdeling Radiotherapie van het UMC Utrecht gewerkt te hebben, is hier dan het resultaat. Zonder de hulp van vele mensen zou dit proefschrift er natuurlijk nooit zo uitgezien hebben. Daarom wil ik bij deze iedereen bedanken die ook maar op enige wijze een bijdrage hieraan geleverd heeft, hetzij door een wetenschappelijke ondersteuning, hetzij door juist een beetje ontspanning naast de promotie te verzorgen. Een aantal mensen wil ik hier graag even noemen.

Als eerste Rien, mijn dagelijkse begeleider. Als ik vragen had, of met een probleem zat, stond jouw deur altijd open. Ook al had je het nog zo druk, je had altijd wel even een momentje om mij weer op weg te helpen. Bedankt voor de goede begeleiding! Verder natuurlijk Jan Lagendijk, mijn promotor. Het hele idee van het ontwikkelen van een robot voor prostaat brachytherapie onder MRI-geleide komt bij jou vandaan. Ondanks dat de ontwikkeling van de robot niet altijd even soepel ging, bleef jij altijd even positief. Bedankt hiervoor. Jan Battermann, mijn andere promotor, wil ik bedanken voor zijn enthousiasme als ik weer met een nieuw idee voor een patiëntenstudie aankwam. Zelfs een naald met een hamer bij een patiënt naar binnen tikken, was geen probleem. Marco van Vulpen wil ik bedanken voor zijn hulp bij het schrijven van de inleiding en natuurlijk voor het inbrengen van een heleboel naalden tijdens het testen van het allereerste prototype van het slagmechanisme. Ook Pieter Hofman heeft nog diverse naalden voor deze studie ingebracht.

De laboranten en doktersassistenten van de brachytherapie wil ik van harte bedanken voor hun hulp bij alle studies die ik gedaan heb. Zonder jullie was het nooit zo goed gegaan!

Natuurlijk wil ik hier ook mijn overige collega's bedanken. Zonder jullie waren

103

de koffie- en lunchpauzes een stuk ongezelliger geweest. Twee mensen wil ik hier even met naam noemen. Met beiden heb ik een kamer gedeeld en met allebei kon ik het op het werk, maar ook buiten het werk altijd goed vinden. Ik vind het dan ook super dat jullie mijn paranimfen willen zijn. Marion en Veronica, bedankt voor alle gezelligheid en steun!

Ook buiten de afdeling Radiotherapie om hebben er nog diverse mensen meegeholpen bij het tot stand komen van dit proefschrift, en dan met name mensen van de afdeling Medische Technologie. Een aantal wil ik hier even persoonlijk noemen. René en Maurits hebben mij beiden geholpen bij het ontwerp van het slagmechanisme. Maurits vooral door het principe erachter uit te werken en René door me te helpen met de kalibratie van de sensor die we gebruikten. Liesbeth heeft het eerste prototype in elkaar gezet. Helaas zal zij het resultaat van haar werk nooit zien. Tenslotte wil ik Ed bedanken. Hij heeft al heel wat tijd in het ontwerp van de robot gestoken, en was altijd even enthousiast, ondanks dat er regelmatig weer onverwachte problemen opdoken. Bedankt voor de samenwerking!

Naast mijn collega' s wil ik natuurlijk ook mijn vrienden en familie bedanken. Voor de gezelligheid die jullie geven, maar ook dat jullie er waren als ik het even niet meer zag zitten. Mijn ouders en mijn zusje wil ik bedanken, gewoon, omdat ze er altijd voor me zijn. Tenslotte, maar zeker niet de minst belangrijke, wil ik Erik bedanken. Natuurlijk voor het ontwerpen van mijn kaft, maar vooral voor de steun en de liefde die ik van je krijg. Ik hoop dat we nog lang samen zullen blijven.

Vera Lagerburg

Curriculum vitae

Vera Lagerburg werd op 6 september 1979 geboren te Middenbeemster. Na acht jaar doorgebracht te hebben op de Bamestra (tegenwoordig Blauwe Morgenster), de plaatselijke lagere school, ging ze naar de RSG (tegenwoordig Jan van Egmond College) in Purmerend. In 1997 behaalde ze hier haar VWO diploma. In september 1997 begon ze haar studie Elektrotechniek aan de Technische Universiteit in Delft, met als specialisatie biomedisch. Haar afstudeerwerk deed ze in het Leyenburg Ziekenhuis in Den Haag, waar ze onder andere onderzoek deed naar automatisch detectie van epileptische aanvallen. Op 1 mei 2003 startte ze met haar promotie onderzoek op de afdeling Radiotherapie van het UMC Utrecht met als doel het ontwikkelen van een robot voor de prostaat brachytherapie onder MRI-geleide. Hier ziet u het resultaat van dit werk. Op 1 juni 2007 is ze begonnen als klinisch fysicus in opleiding (AKF) binnen het samenwerkingsverband tussen het Spaarne Ziekenhuis (Hoofddorp) en het VUmc (Amsterdam).